

The Citrullinating Enzyme PADI4 Binds to Lipids: Identification of New Target Interactions for Cancer Therapy

Salomé Araujo-Abad ¹, Borja García-Peñarrubia ^{2,3}, A. Marcela Giudici ², José L. Neira ^{2,4,*}, Bruno Rizzuti ^{4,5,*}, Camino de Juan Romero ^{2,3,*}, and José A. Poveda ²

- 1 Cancer Research Group, Faculty of Engineering and Applied Sciences, Universidad de Las Américas, 170124 Quito, Ecuador
- 2 IDIBE, Universidad Miguel Hernández, 03202 Elche, Alicante, Spain
- 3 Unidad de Investigación, Fundación para el Fomento de la Investigación Sanitaria y Biomédica de la Comunidad Valenciana (FISABIO), Hospital General Universitario de Elche, Camí de l'Almazara 11, 03203 Elche, Alicante, Spain
- 4 Institute of Biocomputation and Physics of Complex Systems (BIFI), Universidad de Zaragoza 50018 Zaragoza, Spain
- 5 CNR-NANOTEC, SS Rende (CS), Department of Physics, University of Calabria, 87036 Rende, Italy

Correspondence to José L. Neira, Bruno Rizzuti and Camino de Juan Romero: IDIBE, Edificio Torregaitán, Universidad Miguel Hernández, Avda. del Ferrocarril s/n, 03202 Elche, Alicante, Spain (J.L. Neira). CNR-NANOTEC, SS Rende (CS), Department of Physics, University of Calabria, 87036 Rende, Italy (B. Rizzuti). Unidad de Investigación, Fundación para el Fomento de la Investigación Sanitaria y Biomédica de la Comunidad Valenciana (FISABIO), Hospital General Universitario de Elche, Camí de l'Almazara 11, 03203 Elche (Alicante), Spain (C. de Juan Romero). jlneira@umh.es (J.L. Neira), bruno.rizzuti@cnr.it (B. Rizzuti), m.juan@umh.es (C. de Juan Romero) https://doi.org/10.1016/j.jmb.2025.169297

Edited by Georg Schulz

Abstract

Cancer cells need to implement and maintain molecular mechanisms relying on an energy trade-off between resistance and key functions to survive. Among them, changes in lipid metabolism are crucial. Phosphatidylserine (PS), phosphatidylcholine (PC) and phosphatidic acid (PA) are some of the lipids forming cell membranes and having key functions in lipid metabolism. PADI4 is an enzyme implicated in the conversion of arginine to citrulline (citrullination), that has been related with the development of several types of cancers. In this work, we report the lipid binding properties of PADI4. Such binding was assayed in vitro against zwitterionic (PC) and anionic (PA and PS) lipids, and it was monitored by several biophysical techniques. Furthermore, results in silico showed that the binding of PADI4 with PA, PC and PS occurred at the active site of the enzyme. This binding was confirmed in cellulo by using PS as the target lipid, employing immunofluorescence (IF) and proximity ligation assay (PLA) in different cancer cell lines. The use in cellulo of a specific enzymatic inhibitor of PADI4. GSK484, abolished the binding between PADI4 and PS in cancer cells, further indicating that their interaction occurred at the protein active site. Altogether, this work shows that PADI4 was capable of binding to lipids, and opens the venue to study the role that it could be playing in deimination processes and cancer development. Moreover, this study lays the foundation for developing novel cancer therapies from new perspectives, based on the interaction of lipids with citrullinating enzymes.

© 2025 The Author(s). Published by Elsevier Ltd.

Introduction

Cancer cells have an outstanding ability to survive and adapt to harsh microenvironments, such as those characterized by nutrient deprivation and low oxygen levels. The metabolic plasticity of cancer cells is crucial in their adaptative responses to such environments, allowing tumor growth and favoring their resistance to therapy. Recently, research on lipid metabolism of cancer cells has blossomed, and there is evidence that lipid reprogramming in the cell membranes of fastgrowing cancer cells modulates some of the main features of different cancer types [1,2]. For instance, in almost every type of cancer cell the levels of choline are higher than those of their non-malignant counterparts [2]. Choline-containing phospholipids are the most abundant component in the cell membranes of eukaryotes, and phosphatidylcholine (PC) is the predominant phospholipid in most mammalian membranes, constituting 30-50% of all the nuclear lipids. PC is a glycerophospholipid formed by Choline and a phosphate group linked to two acyl chains, either identical or different from each other. In fact, catabolism of PC leads to Choline, diacylglycerol, arachidonic acid and phosphatidic acid (PA), and the latter has pro-tumoral effects, as it is required for cell survival under stress conditions [3,4]. Cancer cells can accumulate many choline-containing metabolites that are breakdown products or, alternatively, precursors of PC. Some of these compounds can exert an intercellular cross-talk under cellular stress conditions, favoring cancer cell growth and resistance to therapy [2].

Phosphatidylserine (PS) is a negatively charged phospholipid, important for the function and integrity of the eukaryotic cell membrane, which is normally asymmetrically distributed in the plasma membrane [5,6]. PS is predominantly found in the inner (cytosolic) leaflet of the membrane bilayer, as Ca²⁺-dependent flippase and scramblase complexes selectively translocate PS inward [7]. However, during cellular activation and/or induction of cell death, PS is moved towards the outer surface of the plasma membrane via the activation of phospholipid scramblases; in fact, it has been shown that PS is often expressed at high levels on the outer leaflet of the plasma membrane of cancer cells [8]. This rise in the amount of PS in cancer cells appears to be related to a decrease of flippase activity, which is associated with an increased influx of Ca²⁺ into cells and oxidative stress responses, observed during chemotherapy and radiotherapy treatments [9,10]. Thus, the identification of cancer cells by the presence of PS on the external surface of the plasma membrane represents an opportunity for selective therapeutic targeting of cancer cells [11]. Whereas the importance of PS in the plasma membrane and in other membrane compartments has been broadly explored, little is known about its

role in the nucleus, although it is known that it contributes to key structural nuclear features by facilitating, for instance, the re-nucleation of the nuclear envelope after cell division [12]. Recently, it has been described that PS is also uniquely enriched in the inner nuclear membrane and nuclear reticulum, where it is critical for supporting the translocation of the proteins CCT α and Lipin1 α [13]. These two enzymes are also important for PC biosynthesis, contributing to its translocation from the nuclear matrix to the inner nuclear membrane and the nuclear reticulum, in response to oleic acid treatment in some cancers [6]. Interestingly enough, PC is predominantly found in the outer (exoplasmic) leaflet of the plasma membrane [6], although there is no specific information in the literature on its location in different types of cancer cells [14.15] Recently, it has been shown that in cancer cells, PC is obtained from lysophosphatidylcholines present in the bloodstream, and by inhibiting the conversion of the those into PC resulted in a decreased tumor growth [16].

PADI4 is a member of the family of peptidylarginine deiminases involved in the conversion of arginine to citrulline residues in a polypeptide chain, in the presence of Ca2+, known as citrullination. Unless the substrate protein is degraded, this post-translational modification is permanent. Citrullination alters the molecular properties of the polypeptide chain, having important roles in human diseases [17-20]. Among other places, PADI4 is usually located in the cytoplasmic granules of eosinophils, neutrophils or macrophages, and in tumor cells, where PADI4 is highly expressed, either in the cytosol or in the nucleus, as we have shown in glioblastoma (GBM), pancreatic adenocarcinoma (PAAD) and colon cancer (COAD) [21]. This enzyme is also involved in gene transcription and immune system modulation [22-26]. In addition, an increase in its enzymatic activity is observed for several PADI4 haplotype mutants during apoptosis enhanced through the mitochondrial pathway [27]. PADI4 also regulates p53 gene expression, as well as the expression of other p53-target genes [26,28,29]. We have recently described the interactions of PADI4 with other macromolecules, showing that PADI4 binds to other key proteins involved in cancer development, such as importin α3, plakophilin 1 (PKP1), murine double minute 2 (MDM2), the nuclear protein 1 (NUPR1), RING1 and YY1binding protein; and the Really Interesting New Gene protein 1B (RING1B) [30-35].

In this work, we investigated the binding between several types of lipids and the citrullinating enzyme PADI4. Our studies were prompted by the fact that: (i) some members of PADI family can be involved in intracellular energy metabolism [36]; and (ii) we were scanning proteins with some disordered regions which could interact with lipids by using several on-line prediction servers [37]

(Section 'Bioinformatic analysis identifies potential hot-spots for PADI4 interaction with lipids'). We showed the interaction in vitro of this enzyme with brain PS (bPS), egg PC (ePC), POPA (1palmitoyl-2-oleoyl-sn-glycero-3-phospahtidic acid (sodium salt)) and POPC (1-palmitoyl-2-oleoyl-snglycero-3-PC), by using several biophysical and spectroscopic techniques. In cellulo, we reported the binding between PADI4 and PS at the inner nuclear membrane of cancer cells. This interaction was abolished in cellulo by using a specific enzymatic inhibitor that targets the catalytic pocket of PADI4, namely GSK484. Molecular simulations confirmed that the binding occurred at the active site of the enzyme, thus contributing to rule out the possibility of an allosteric binding of lipids to PADI4, and providing a molecular model for the protein/lipid interaction. This study raises new questions about the role that PADI4 and its interactions with other macromolecules could have in cancer progression. Interestingly, the binding of different kinds of lipids to PADI4 opens the venue to study other mechanisms of the action this enzyme, specifically related to PS within the inner nuclear membrane, highlighting additional pharmacological possibilities for targeting several types of tumors.

Results

Lipids bind in vitro to PADI4 independently of their charge

Many signaling cascades begin with the generation of bioactive lipids or, alternatively, precursors of them (such as PA or Choline), that recruit downstream effectors and modulate their enzymatic activity. Then, to test for the possible binding between PADI4 and lipids, we assayed large unilamellar vesicles (LUVs) containing those headgroups (namely, Choline and PA). Moreover, to show that the interaction is not lipid-chargedependent. we used lipids with electrostatic properties. Therefore, we studied the binding of PADI4 in vitro with: (i) ePC, which is a zwitterionic lipid; and (ii) PA and PS, which are both anionic. However, since under homeostatic conditions PS is restricted to the inner leaflet of the membrane, accounting for a small proportion of the total amount of lipids (smaller than 2%), we decided to use as an in vitro model for testing the binding of PS to PADI4 LUVs formed by the mixture of ePC (75% w/w) and bPS (25% w/w).

We first used fluorescence lifetime and steadystate anisotropy of the protein to measure the interaction between the different LUVs and PADI4. Since PADI4 has ten tryptophan residues distributed through its primary structure, it could be expected that, in the best possible scenario, its intrinsic fluorescence could monitor the interaction of the enzyme with the LUVs. Therefore, a fixed amount of PADI4 was diluted in buffer and its emission spectrum, fluorescence lifetime, and steady-state anisotropy were measured while amounts of the above indicated lipids were added. Neither the emission spectrum fluorescence lifetime was modified upon lipid addition (Suppl. Figures 1 and 2). However, the anisotropy, <r>, decreased as LUV concentration was raised (Figure 1 A). This decrease in anisotropy with either the zwitterionic ePC or the anionic ePC/bPS vesicles is indicative of lipidprotein interactions. The value of <*r*> depends on: (i) the global and local rotation movements of the protein; (ii) possible homo-Förster-resonance-ener gy-transfer phenomena among the different tryptophan residues; and, (iii) individual tryptophan fluorescence lifetimes. Unfortunately. molecular interpretation of these anisotropy changes in a protein with such a high number of tryptophan residues in PADI4 is not possible.

Despite these limitations, our findings revealed that PADI4 could interact with both membranes, i.e. a zwitterionic one such as ePC, and an anionic one (ePC/bPS), suggesting that the binding process was not primarily ruled by electrostatic forces. Furthermore, the similar values of the final anisotropy of PADI4 in the various experiments suggested that the protein conformation when bound to each of the LUVs could be similar (Figure 1A).

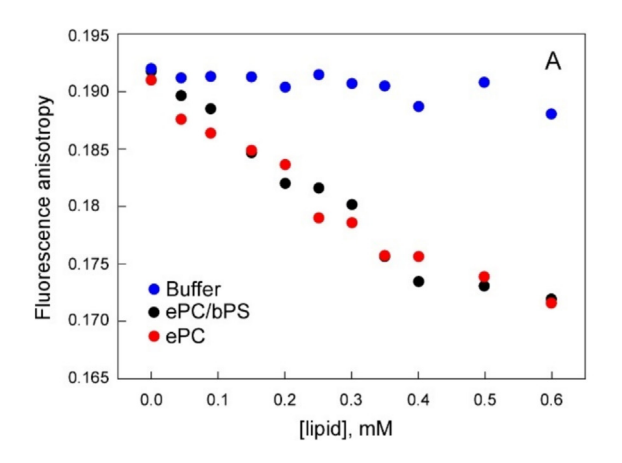
Lipid aggregation assay further supported the binding of PADI4 to lipids

To further investigate the binding of two lipid species (PA and PC) to PADI4 *in vitro*, we next examined the effect on the aggregation of the former upon addition of increasing amounts of the enzyme.

Based on the measurements of scattered light, the aggregation assays allowed us to test the possible changes that the PADI4/lipid interaction could produce on the lipid membrane structure. For this type of experiment, two standard types of lipids were used, either a zwitterionic lipid (POPC) or an anionic one (POPA). We used these two LUVs, instead of the other two assayed in the anisotropy measurements, to ensure that the type of the fatty acid chain present in the lipid was not responsible for the binding to PADI4 (Figure 1 B).

The addition of the protein to both kinds of LUVs induced a large light scattering, indicating an increase in the size of the lipid vesicles. In the case of zwitterionic POPC, the process followed a hyperbolic curve (Figure 1 B), whereas for the anionic POPA, the sample became cloudy and the scattered light decreased, which is typical of lipid aggregation into larger structures resulting in Mie scattering [38]. This process of aggregation of POPA was relatively slow, since the scatter signal was greatly reduced after 30 min, making difficult its quantification.

Altogether, the scattering observed in the lipid samples indicated that, from the lipid "point of



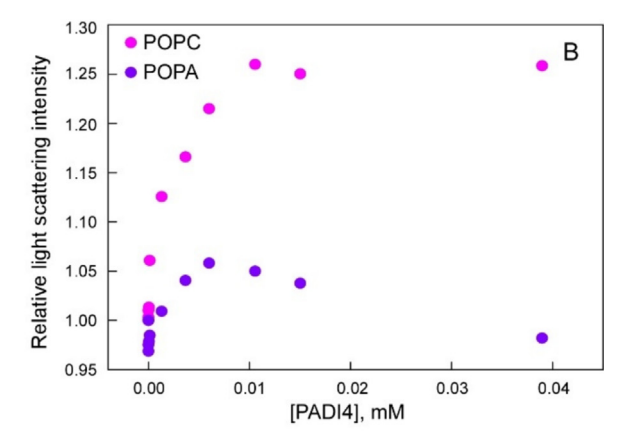


Figure 1. PADI4 binding to lipid membranes. The binding of PADI4 to lipids was followed by fluorescence anisotropy (A) and light scattering (B). Increasing amounts of lipid were added to a fixed amount of PADI4, and the intrinsic steady-state fluorescence anisotropy of the protein was measured. Background signal from the lipid is corrected by using a sample with no protein. A control sample experiment, where buffer, instead of lipid, was added to PADI4 is shown for comparison in (A). Increasing amounts of PADI4 were added to a fixed amount of lipid vesicles, and the scattered light was measured. Data are expressed as the ratio of scattered light relative to that of the sample with no added protein (B).

view", there was binding with the enzyme; furthermore, the binding was not fatty-acid-chain dependent, since the LUVs used had a single fatty acid chain. Moreover, these findings reinforced the observation that the binding was not lipid-charge dependent.

BLI assays in the presence and absence of an inhibitor of PADI4

Assays in the absence of GSK484. After proving the binding between the enzyme and the lipids from the "point of view" of both macromolecules, we quantitatively measured the kinetic parameters of such binding, by using biolayer interferometry (BLI) (Figure 2A). As in the anisotropy measurements, in the BLI experiments we used LUVs made of pure zwitterionic ePC, or a mixture with the anionic bPS (75% w/w of ePC and 25% w/w of bPS).

For ePC, the range of explored concentrations was 13.8 to 1.8 mM. In all cases, the association curves (of PADI4 to the lipids) did not reach a plateau (Figure 2A). The lack of an equilibrium does not invalidate the use of Eqs. (2) and (3) (Section 'Experimental design of the BLI experiments in the presence of GSK484'), as the only equilibrium parameter in such equations is R_{eq} , reached at virtually infinite time when dR(t)dt = 0, and this parameter is always determined from the data fitting. The use of $R_{\rm eq}$ to determine the equilibrium constant, K_d , corresponds to a strict thermodynamic approach, and it can be applied even though equilibrium has not been attained during the experiment [39]. In our interpretation of the results of the binding of PADI4 to the

lipids, we did not use the calculated values of $R_{\rm eq}$. In the analyses of the data, either ePC or ePC/ bPS, we included the term describing a straight line (the slope at the largest association times), $R'_{eq}(t-t_0)$, in the fitting of the exponential curve, to account for the linear variation observed at times close to 300 s, which is clearly non-exponential. That behavior does not invalidate the use of Eq. (4) (Section 'Experimental design of the BLI experiments in the presence of GSK48'); in fact, Eq. (4) takes into account the non-exponential behavior observed in the experiments at the largest association times. However, since only the exponential section of the sensorgram is important for the pseudofirst order plot, the presence of this linear term does not alter the result for any of the lipids; furthermore, the slopes are in the range of $1-5 \times 10^{-6} \, \text{s}^{-1}$ for all the lipid concentrations. When setting up our experimental conditions at the beginning of all the experimental work, we explored association times of 180 and 200 s, instead of 120 s; in all cases we observed a slope of the curve at the longest association times. The 120 s time we used during the association step was a compromise among: (i) the total acquisition time during the experiment; (ii) the association time of the lipid to the biosensorattached PADI4; (iii) the avidity effects; and (iv) the possible unspecific binding of the lipid in the solution to the biosensor (as it is indicated in the manufacturer instructions).

The pseudo-first order plot yielded (Figure 2B) a value of $k_{\rm on} = 0.041 \pm 0.004 \ {\rm mM}^{-1} \ {\rm s}^{-1}$. The value of $k_{\rm off}$, the y-axis intercept in the pseudo-first order plot, was negative; however, from the dissociation step, we were able to obtain a value of $k_{\rm off} = 0.28 \pm 0.17 \ {\rm s}^{-1}$ (Suppl. Figure 3A). Therefore, by assuming that, from a kinetic point of view, the

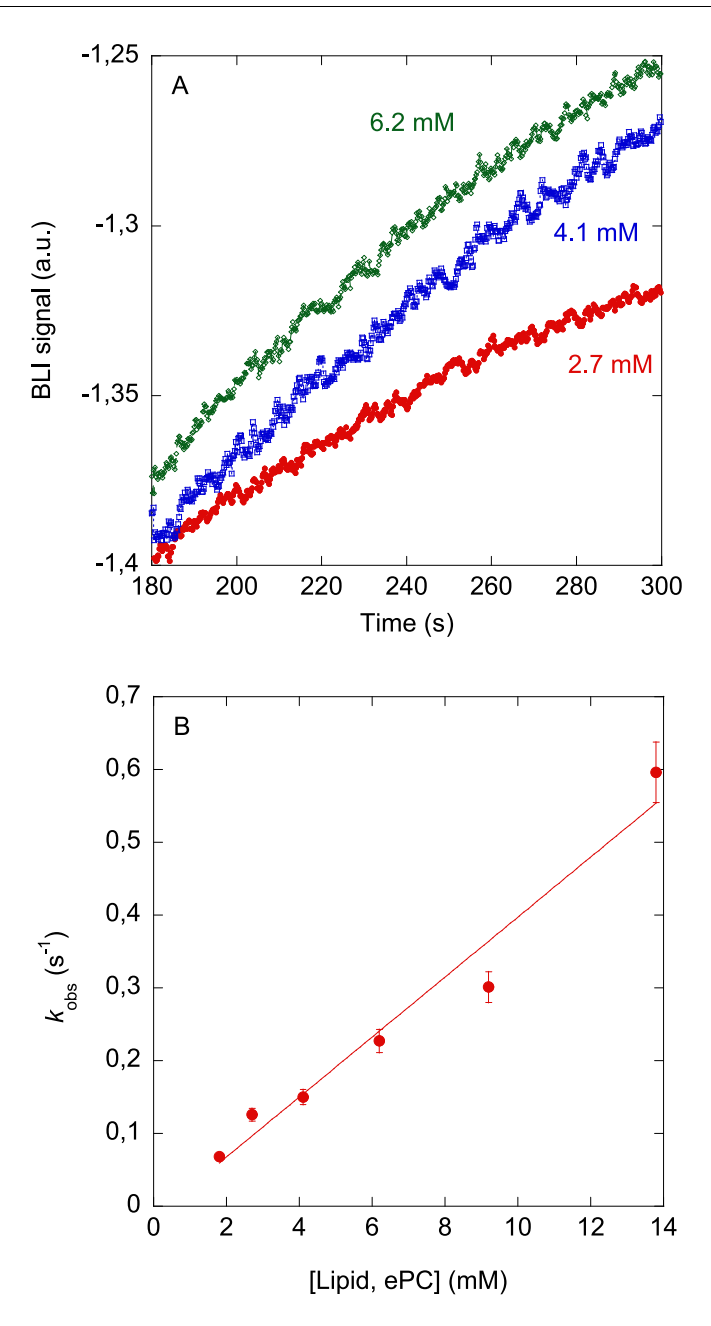


Figure 2. Affinity of ePC towards PADI4 as monitored by BLI assays. (A) Sensorgrams for the association step at different concentrations of ePC used in the assays for biosensor-immobilized PADI4 in the absence of GSK484. (B) Pseudo-first order plot of the binding of ePC to PADI4 corresponding to the curve with the exponential with the largest k_{obs} value (Eq. (5)). The error bars are uncertainties from fitting sensorgrams to Eq. (4). All experiments were carried out at 25 °C.

process is two-state, we obtained an apparent dissociation constant of 6 ± 2 mM.

The range of concentrations explored for the ePC/bPS was 1.7–5.9 mM. In this case, as it happens with the ePC lipid described above, the sensorgrams in the association process did not reach a plateau (Figure 3A). The pseudo-first order plot yielded a value for the apparent dissociation constant of 1.0 \pm 0.5 mM (Figure 3B), with $k_{\rm on}$ = 0.019 \pm 0.03 mM⁻¹ s⁻¹ and $k_{\rm off}$ = 0.02 \pm

0.001 s⁻¹ (conversely to what happens for the ePC). This value of the k_{off} rate was smaller than that obtained from the dissociation section of the sensorgram: $k_{\text{off}} = 0.072 \pm 0.008 \text{ s}^{-1}$ (Suppl. Figure 4A).

The apparent values of these dissociation constants are within the same range (1–3 mM) obtained with the C-terminal region of the sterile alpha motif domain of p73 when they are bound to PC or PA LUVs [40].

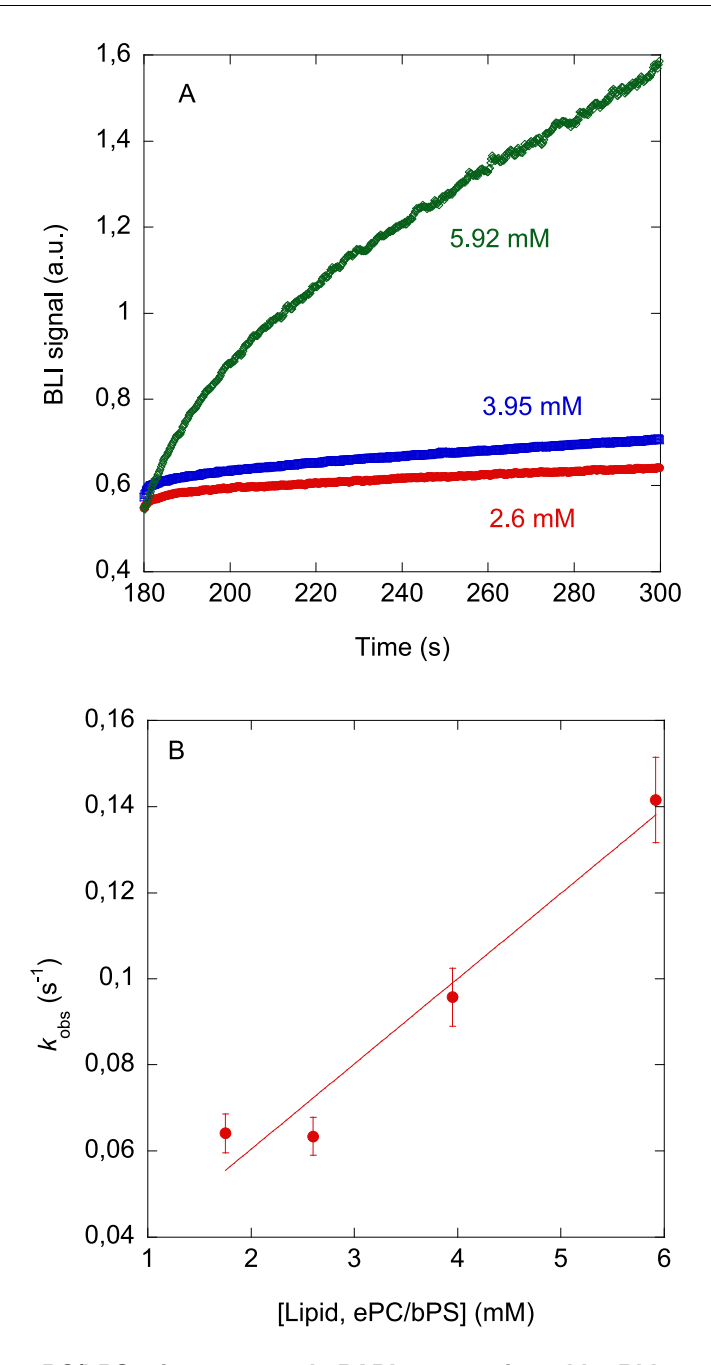


Figure 3. Affinity of the ePC/bPS mixture towards PADI4 as monitored by BLI assays. (A) Sensorgrams for the association step at different concentrations of the mixture of ePC/bPS used in the assays for biosensor-immobilized PADI4 in the absence of GSK484. (B) Pseudo-first order plot of the binding of ePC/bPS mixture to PADI4 corresponding to the curve with the exponential with the largest $k_{\rm obs}$ value (Eq. (5)). The error bars are uncertainties from fitting the sensorgrams to Eq. (4). All experiments were carried out at 25 °C.

Assays in the presence of GSK484. Next, we tried to quantitatively measured the kinetic parameters of the binding of PADI4 to lipids, by using BLI in the presence of saturating concentrations of GSK484. As above, we used LUVs made of zwitterionic ePC, and anionic bPS (a mixture of 75% w/w of ePC and 25% w/w of bPS).

For ePC, the range of lipid concentrations was from 1.8 to 8.0 mM, in the presence in all cases of

110 μ M of GSK484. In this case, the sensorgrams in the association step of ePC in the presence of the biosensor-attached PADI4/GSK484 complex did not show the typical exponential behavior but rather a more complex tendency (Suppl. Figure 5A) indicating the presence of several concomitant association and possibly dissociation steps. Therefore, we could not obtain a pseudo-first order plot, neither did we obtain the $k_{\rm on}$ rate.

On the other hand, the dissociation step in the sensorgrams from the biosensor-attached PADI4/GSK484 complex showed the typical tendency of an exponential behavior (Suppl. Figure 3B), from where a $k_{\rm off}$ rate of 0.38 \pm 0.23 s⁻¹, similar to the one obtained in the absence of the GSK484.

For the experiments with ePC/bPS, the range of lipid concentrations was from 1.16 to 7.6 mM, in the presence in all cases of 110 µM of GSK484. Although, the sensorgrams in the association step of ePC/PS to the biosensor-attached PADI4/ GSK484 complex did show an apparent exponential behavior, when we tried to find the curves, we could not fit the data to Eq. (4). Instead, data were better fitted to a one exponential, where a Langmuir term is included: $R(t) = R_{eq} - R_{eq} e^{(-k_{obs}(t-t_0))} - \frac{R''_{eq}}{t} - R''_{eq}(t-t_0)$ (Suppl. Figure 5B). These findings, together with those observed for ePC in the presence of the inhibitor, indicate that GSK484 was affecting the lipid/PADI4 binding.

The dissociation step of the lipid in the sensorgrams from the biosensor-attached PADI4/GSK484 showed also a behavior different (Suppl. Figure 4B) to that observed for ePC lipid (either in the absence or in the presence of GSK484, Suppl. Figure 3B), as they could not be fitted to Eq. (6), but they rather could be fitted to a modified equation, that also included a Langmuir term: $R(t) = R_1 e^{(-k_{off}(t-t_0))} - R_2(t-t_0) - R_3/t$.

Therefore, our results with BLI indicate that: (i) there was binding between PADI4 and the two kinds of lipid (thus confirming the results of fluorescence and scattering); and, (ii) the presence of the GSK484 altered the binding of the lipid to PADI4, showing sensorgrams with a behavior different to that currently observed when there is binding (Supplementary Figure 5 A), and making necessary the addition of a further term in the fitting (Supplementary Figure 5B). These results suggest that the lipid could compete for the binding to the active site with the inhibitor, or alternatively, that the lipid could bind to an allosteric site which would affect the conformation of the active site.

The presence of the lipids hampered citrullination of N-α-benzoyl-L-arginine ethyl ester in vitro

We carried out color development reagent (COLDER) experiments to elucidate whether the presence of the lipid would hamper the citrullination of N- α -Benzoyl-L-arginine ethyl ester (BAEE), a substrate for PADI4 [41]. Furthermore, we also carried out experiments in the presence of antipyrine and an oxime [42].

Our results with the two-colored reagents show, more clearly in the experiments based on the addition of antipyrine, that in the presence of either ePC (Suppl. Figure 6) or ePC/bPS (Suppl. Figure 7), the citrullination of BAEE did not occur

so effectively as when only PADI4 was present in solution. This decrease in color, indicating a lower amount of citrulline formed in the reaction and less absorbance in the UV spectra, was not as important when the lipids were in the solution, as when the GSK484 was present, but it was still observed (better observed when antipyrine was used as reagent). That is, both lipids hampered the citrullination of BAEE, but not as efficiently as GSK484. Moreover, this decrease in the activity of PADI4 upon lipid addition was larger for ePC than for ePC/bPS, as judged by the more intensity of the colored samples in the latter (more clearly in the experiments based on the addition of antipyrine). Therefore, we suggest that both lipids could bind to the active site of the enzyme, confirmina the findings observed experiments in the presence of GSK484, although we cannot unambiguously rule out the presence of an allosteric effect triggered by the lipid in the protein.

Bioinformatic analysis identifies potential hotspots for PADI4 interaction with lipids

To elucidate how PADI4 can bind lipids and which are the specific protein-interacting regions, we used the method developed by White and Wimley [43], allowing us the identification of the putative protein-membrane interacting regions. Using windows of either 7, 9, or 11 amino acids in the sequence analysis, this approach showed that four segments of the protein, those comprising residues Leu254-Leu272, Ala282-Pro300, Ala581-Pro599, and Pro622-His640, were thermodynamically favored to be in contact with both the hydrophobic hydrocarbon core and the membrane interfacial region and, therefore, could represent hot-spot regions for PADI4/lipid interaction.

Figure 4 shows where these regions were located in the structure of the PADI4 dimer. The segment Leu254-Leu272 is in the central region of the homodimer. In principle, this region is accessible to lipids, but more likely to single isolated lipid molecules rather than to a membrane - even a relatively small one. In fact, this region is in the groove of the PADI4 dimer, and it could become exposed to a relatively flat lipid layer only upon dissociation of the two monomers, which was not observed in our experiments. For a similar reason, also the fragment Ala282-Pro300 could be excluded as a hot-spot region of PADI4 for lipid binding. In fact, although in principle its sequence has the typical features that are favorable to bind lipids, it is almost completely buried below the surface of each PADI4 monomer. Therefore, it is not accessible to lipids (neither isolated nor organized in a layer), unless there is an unfolding of the tertiary structure of the monomers, which does not take place in our steady-state fluorescence experiments (data not shown). This leaves the other two regions Ala581-Pro599 and

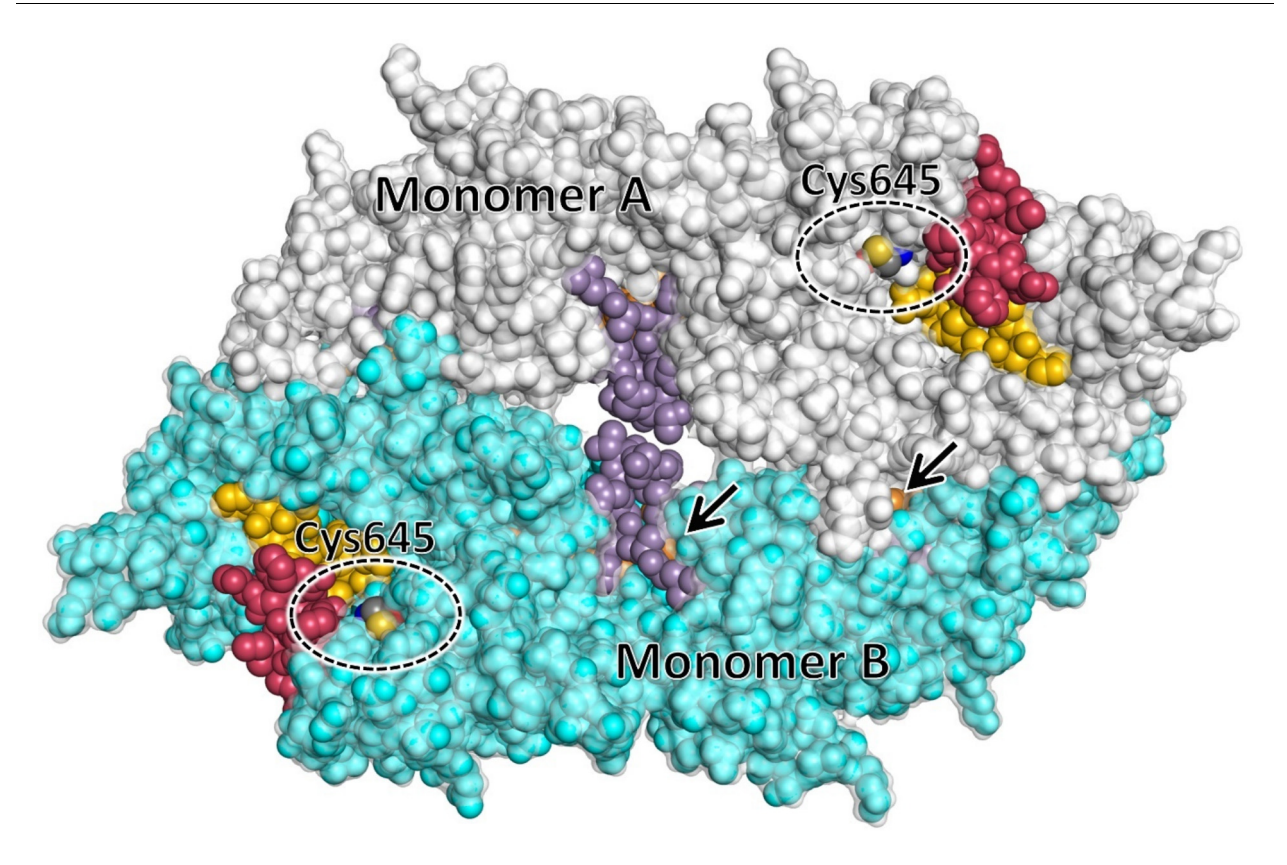


Figure 4. Potential hot-spots of PADI4 for the interaction with lipids. Putative PADI4/membrane interacting regions obtained in the bioinformatic analysis: residues Leu254-Leu272 (purple), Ala282-Pro300 (orange), Ala581-Pro599 (yellow), and Pro622-His640 (red). Region Ala282-Pro300 is mostly buried, and a few visible atoms corresponding to this region are indicated in each of the monomers (arrows). The key catalytic residue Cys645 in the active site is also labeled (circled). The two monomers of PADI4 are in different colors (white and cyan).

Pro622-His640, which are both close to the active site of PADI4, as those that are the most likely to interact with lipids.

Structural prediction of the PADI4/lipid binding

Molecular docking was used as a further computational methodology to predict the binding region of lipids to PADI4. This technique is difficult to apply to phospholipids, due to their large number of rotational degrees of freedom (≥36 rotatable bonds in our case, see Table 1). Therefore, we used the innovative algorithm DiffDock [44], which is less sensitive to such limitation, and represents an efficient and accurate improvement over traditional methodologies [45].

We performed a blind docking of our three lipid molecules (PS, PC, and PA) on the dimeric structure of PADI4, predicting their interaction without presuming any bias on the preferred protein binding region (Figure 5). In all the docking poses (40 binding modes for each lipid species), the ligands were invariably found with the headgroup clamped in between residue Val469 and the key catalytic Cys645 of PADI4. These results further support the findings obtained in the

colorimetric reactions (Suppl. Figure 6 and 7), and in the BLI experiments in the presence and in the absence of GSK484 (Suppl. Figures 3, 4 and 5). The two aliphatic chains of the lipids interacted each with one of the two main regions identified in the hydropathy analysis of the protein sequence (Section 3.3): residues Ala581-Pro599 Pro622-His640, and especially with the latter. Although the simulations were performed with a single lipid molecule, no docking pose was observed to bind in the central region of the homodimer, that is, with the protein fragment Leu254-Leu272; although this region was described as potentially accessible to an isolated lipid molecule in the previous bioinformatic analysis (Section 2.5). The only other binding region identified in the previous analysis (Ala282-Pro300), was also not targeted by the lipids in the simulations because it is sterically inaccessible.

We also performed an MM/GBSA analysis of the best binding modes obtained, to estimate the approximate binding free energy of the lipid molecules and to better identify the anchoring hotspot residues of PADI4. The findings reported in Table 1 indicate very favorable binding affinities (energy < -40 kcal/mol). Several aromatic

Table 1 MM/GBSA analysis of the most favorable PADI4/lipid complexes obtained by molecular docking.

Lipid	Charge	Rotatable bonds	Binding free energy (kcal/mol)	Anchoring protein residues ^a
Phosphatidylserine (PS)	-1 (anionic)	37	-49.8 ± 5.4	Phe634 (-1.69), Tyr636
				(-1.64),
				Val469 (−1.57),
				Gly408 (-1.47),
				Cys645 (-1.14)
Phosphatidylcholine (PC)	0 (zwitterionic)	41	-40.6 ± 5.3	Tyr636 (-1.62),
				Phe633 (-1.28),
				Phe634 (-1.24),
				Cys645 (-0.98),
				Val469 (-0.96)
Phosphatidic acid (PA)	-1 (anionic)	36	-47.6 ± 4.4	Tyr636 (-1.48),
				Phe582 (-1.17),
				Val469 (−1.08),
				Phe633 (-1.10),
				Phe634 (-1.07)

^a Protein residues with the most favorable binding affinity for the lipids (values in kcal/mol are in parentheses).

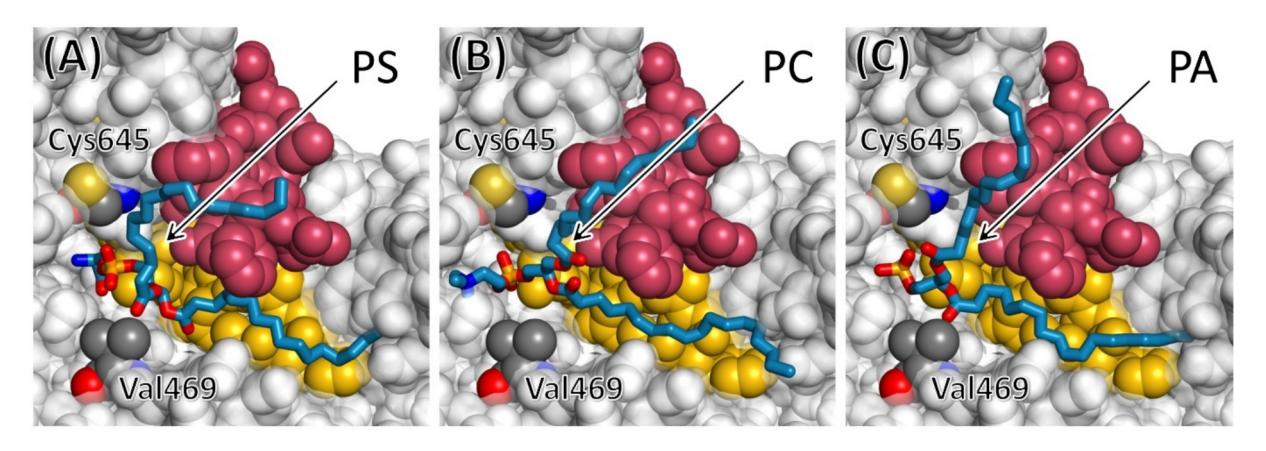


Figure 5. Most favorable docking poses of the lipids on the surface of PADI4. Binding modes were predicted in correspondence with the PADI4 catalytic site, for (A) phosphatidylserine (PS), (B) phosphatidylcholine (PC), and (C) phosphatidic acid (PA). Residues Val469 and the key catalytic residue Cys645, clamping the lipid headgroups, are labeled. Regions Ala581-Pro599 (yellow) and Pro622-His640 (red), predicted by the bioinformatic analysis to bind the two lipid alkyl chains, are also shown.

residues contributed to anchoring the lipids on the protein surface (energy ≤ -1 kcal/mol), and in particular, the small hydrophobic patch including residues Phe633, Phe634, and Tyr636, which was already found to be crucial in the interaction of PADI4 with partner proteins such as MDM2 and RYBP [33,34].

In summary, the overall simulation results indicate a clear tendency of all the lipids to interact with the same PADI4 location (i.e., the protein active site), and with a mutually common binding mode – although the details depend upon each lipid species. These structural details observed *in silico* could mimic the different behavior of the two lipids in the BLI experiments (Section 'BLI assays in the presence and absence of an inhibitor of PADI4'). Even though the docking predictions could only prove the anchoring of a single isolated molecule, once a first lipid is bound in the

(constrained) predicted conformation, it could encourage the spontaneous arrangement of further lipids in the same location. The possibility of binding of more than one lipid molecule is also supported by the previous bioinformatic analysis, which mimics the free energy of transfer of the two key protein regions, evidenced in the docking simulations (Ala581-Pro599 and Pro622-His640), to the hydrocarbon core of a membrane bilayer.

PADI4 and PS were differently expressed in tumor and non-tumor cells

After showing the binding *in vitro* between PADI4 and different model LUVs, which could mimic the membrane cell, we tested whether such binding occurred also *in cellulo*.

The distribution and dynamics of PS in the nuclei of intact cells have already been investigated by using PS biosensors, showing a PS enrichment in

the inner nuclear membrane and nuclear reticulum of U2OS cells [13]. To label the PS in the intracellular compartments, we permeabilized different cell types to allow for the access to the inner nuclear membrane. This was important as the interaction was expected to occur near the nucleus, where PADI4 is predominantly expressed, although it has been reported that its expression varies depending on the cell line (i.e. GBM, PAAD and COAD) [21].

As PS has been shown to be differently distributed along the plasma membrane of cancer and healthy cells, we speculated that it may also differ in the inner nuclear membrane [8]. Therefore, we studied the expression of PADI4 and PS in cancer cells (namely, HGUE-GB-42 and SW-480) and non-tumor cells (HEK and MRC-5). For GBM, we used a previously described patient-derived cell line, HGUE-GB-42 [46]. And for colorectal cancer, we used SW-480, isolated from the large intestine of a Dukes C colorectal cancer patient. On the other hand. for non-cancerous cell lines, we used: (i) MRC-5, a cell line established from normal lung tissue of a 14-week-old male fetus; and (ii) HEK-293, a human embryonic kidney cell line. It has been previously reported that the expression of PADI4 depends on the cell line, resulting in a different PADI4 localization; hence, the chosen cell lines were from different tissues, to cover as much as possible a wide range of likely distributions of this protein [21].

First, we performed immunofluorescence (IF) experiments to determine whether PS and PADI4 colocalized in the inner nuclear membrane of those cell lines (Figure 6 and Suppl. Figure 8). We found that PADI4 was highly expressed in the nucleus and cytoplasm of HGUE-GB-42, as previously reported [21], but also in the other cell lines examined, as shown by the colocalization with DAPI (4',6-diamidino-2-phenylindole), a fluorescent dye that binds DNA and is used to label cell nuclei (Figure 6). Since all the cells were permeabilized, we were able to observe PS expression in the inner nuclear membrane. Interestingly, the distribution of PS was dependent on the cell line. Whereas in cancer cells PS expression was mostly restricted to the nucleus and showed an asymmetric distribution, even within the same cell type, in non-cancer cells PS was also present in the cytoplasm (Figure 6 and Suppl. Figure 8).

PADI4 and PS interacted in cellulo in the nucleus of cancer cells

Our findings suggested that PADI4 and PS might interact within different cell compartments depending on the cell line, which prompted us to seek confirmation of their binding by using the Duolink In situ assay. This technique, known as proximity ligation assay (PLA), resolves protein binding that occurs at distances shorter than 16 Å. The observed red fluorescent spots,

corresponding to the PLA signals, indicated that PADI4 efficiently interacted with PS in all cell lines (Figure 7A). In agreement with the immunocytochemistry results, we observed that in the used cancer cells the interaction of PADI4 with PS was located at the nucleus, whereas in noncancer cells it took place mostly in the cytoplasm (Figure 7A).

Our results showed that PADI4 could bind to PS *in cellulo*. This interaction varied between tumor and non-tumor cells, and this was clearly related to the fact that PS is distributed differently in healthy cells, as compared to pathological ones. A difference in PS distribution on the plasma membrane between cancer and non-cancer cells has been described [6,47,48]; however, this is the first time that such a difference has been reported close to the inner nuclear membrane. Furthermore, this difference in the PS content affected the binding of PS to PADI4 (Figure 7A).

In silico results indicated that the active site of PADI4 was involved in the interaction with the lipid, therefore we used the PADI4 specific inhibitor GSK484 in cellulo to validate these findings. PLA experiments showed a slight decrease in the interaction after 1 and 3 h of treatment, whereas after 6 h in the presence of the inhibitor the PADI4/PS interactions in HGUE-GB-42 cells were completely abolished (Figure 7 C). These results further support the fact that PADI4 and PS were interacting through the active site of the enzyme, in agreement with the in silico results and the findings of the colorimetric and BLI assays. Furthermore, these findings open new possibilities for acting on cancer progression by hampering or modulating this interaction with the use of PADI4 inhibitors.

Discussion

Lipid metabolism is a key cellular process, involving the synthesis, utilization, and degradation of these molecules. In cancer cells, lipid metabolism is modified to ensure the fast growth rates and high energy demands in the harsh environments in which they proliferate. In addition to being a source of energy, lipids are also important signaling molecules in cancer. In fact, cellular membrane components such as phosphoinositides, eicosanoids, and sphingolipids, are all involved in cell growth, differentiation, apoptosis and stress responses [47,49].

In all tissues, glycerophospholipids constitute the most abundant class of lipids. The largest fraction of them is represented by PC, and the smallest, but significant, by PS, although glycerophospholipid fingerprint varies among the cells and the environmental conditions. Considering: (i) the movement of PS from the inner leaflet towards the outer section of the membrane during the triggering of cell death; and, (ii) the elevated

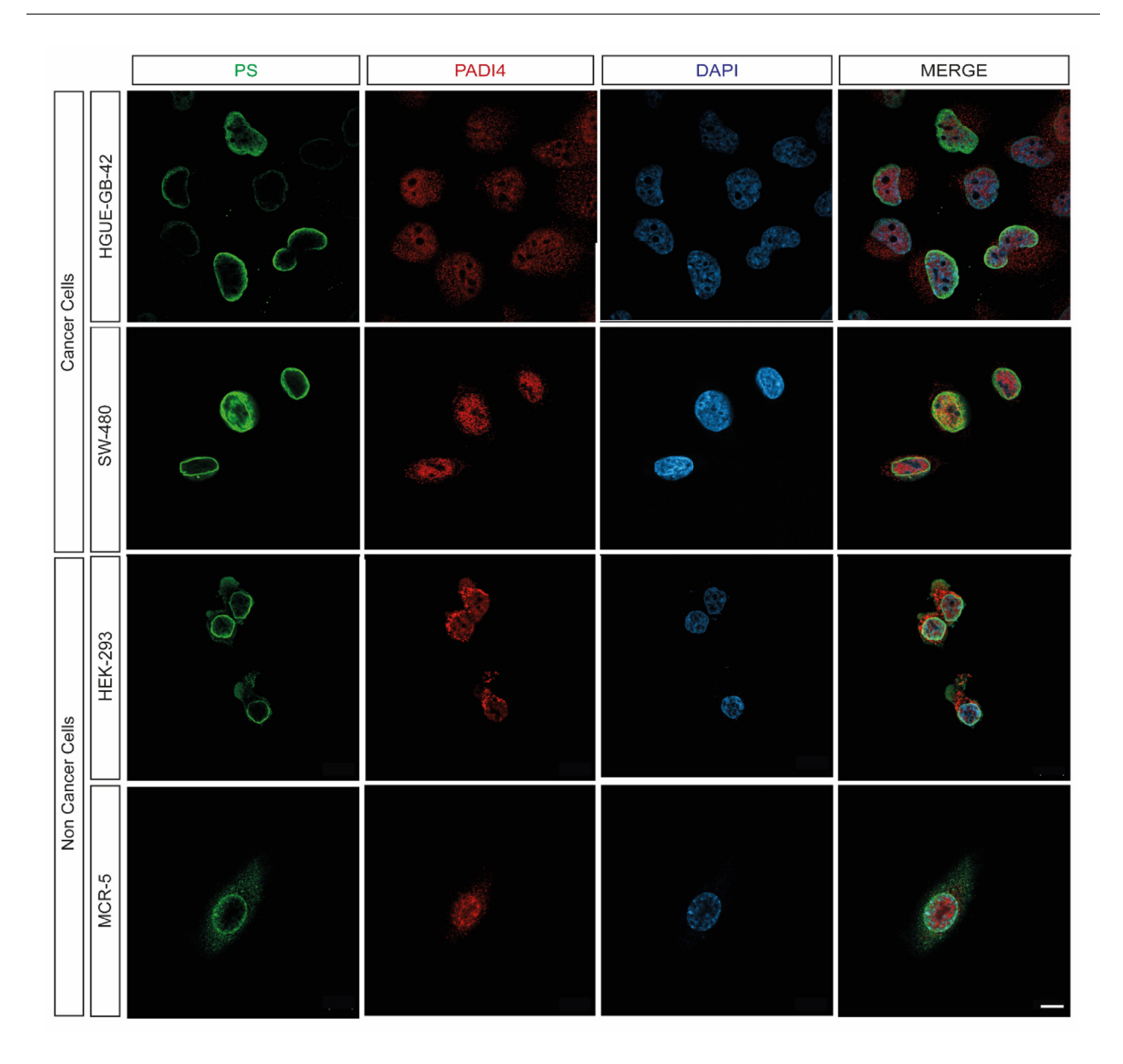
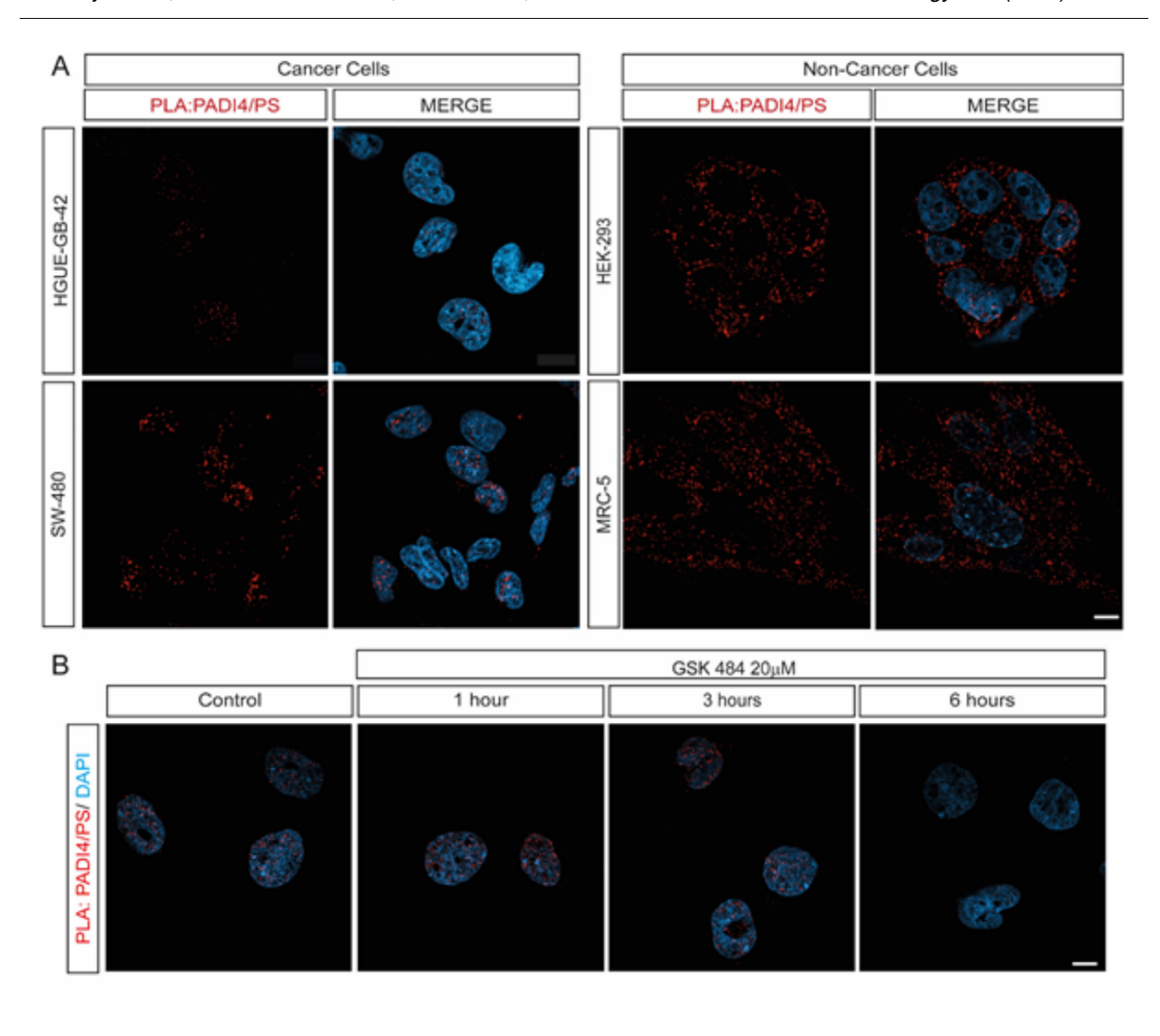


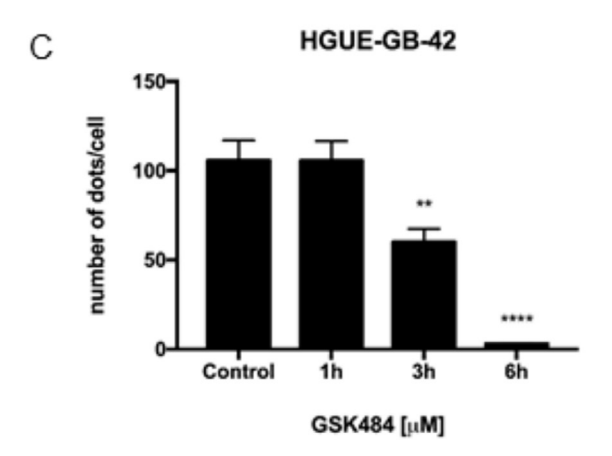
Figure 6. Immunofluorescence of PADI4 and phosphatidylserine (PS). PADI4 (red), PS (green) and DAPI (blue) in cancer cell lines (HGUE-GB-42 and SW480) and non-cancer cell lines (HEK-293 and MCR5). Scale bar: $10~\mu m$.

content of Choline-containing lipids in cancer cells, it is safe to assume that cancer cells have efficient modulation of lipidic contain to sustain those changes and that there should be interactions of lipids with several proteins involved in cancer progression. Although the plasma membrane of their associated cancer cells and tumor vasculature exhibit high levels of PS on the outer leaflet, this externalized phospholipid has not been associated with apoptosis [50]. It has been shown that the specificity of abundant externalized PS for malignant tumors, including metastatic melanoma and metastatic lesions, could be considered as a reliable biomarker for both primary and metastatic tumors [51]. Furthermore, the presence of PS at the external region of the inner nuclear membrane

has been poorly studied in cancer cells. In this work, we showed *in vitro*, *in silico*, and *in cellulo* that PS interacted with PADI4, a protein that could be translocated into the nucleus [9], and which is involved in the citrullination of several nuclear proteins [34,35].

Binding of PADI4 to lipids was not lipid-charge-dependent. Furthermore, such binding did not result in significant structural tertiary modifications around the tryptophans or tyrosines of the protein, as judged by the absence of changes in the emission spectra and lifetimes measurements of the tryptophans (Suppl. Figures 1 and 2). These results are not surprising since PADI4 is a protein with a pI of 6.15, and with a large compact structure burying a hefty amount of hydrophobic





surface. From our computational findings, it is evident that all the types of lipids bind to the PADI4 active site, with the headgroup close to the key catalytic residue Cys645, and with each of their two alkyl chains interacting with the two main regions (Ala581-Pro599 and Pro622-His640) identified in the bioinformatic analysis of the hydrophobic properties of the protein sequence. The former of those two regions includes the aromatic residues Phe582, Phe583, and His595, whereas the latter includes Phe629, Phe633, Phe634, and Tyr636, some of which could contribute to the changes detected in the steadyanisotropy measurements of (Figure 1A). In particular, the docking simulations suggest a significant contribution of the protein patch Phe633-Tyr636 to the lipid binding, as it happens for other molecular partners of PADI4 [33,34]. The conformational changes suffered by the aromatic-rich protein fragments of PADI4 must not be very dramatic, however, since upon lipid binding the tertiary organization of the protein was not substantially altered, as shown by the steadystate fluorescence spectra (Suppl. Figure 1). The aromatic residues of PADI4 represent a first anchoring point for the lipids and, as suggested by the bioinformatic analysis, would locate in the interfacial region of the membrane in the case several lipid molecules concur to the binding, influencing their precise interfacial positioning. The curves obtained in the anisotropy measurements (Figure 1A), in contrast with ones from the aggregation assays (Figure 1B), indicate that the lipid-protein interaction causes quite complex binding equilibria in the protein, probably including concomitant conformational changes and/or protein-protein and protein-lipid interactions. The existence of these different equilibria could be further supported by the observations made in presence of GSK484, which seems to alter the mode of binding of the lipid to the biosensor-attached PADI4/GSK484 complex. The fact that the lipid-saturation observed in the fluorescence curves does not agree with the determined dissociation constant from BLI experiments, under the conditions where it was possible, further suggest that the binding process is not a two-state one from the kinetic point of view.

We do not know the exact process by which the scattering of the lipid occurs, but dynamic light scattering measurements with the PC/PS mixture show a complex mechanism with a high heterogeneity of the lipid/PADI4 mixture (data not shown). The fact that saturation, in the scattering measurements (Figure 1B), occurs lower than the concentrations dissociation constant determined by BLI could be due to the assumption that binding is a two-state process. Furthermore, the observation that the two lipids showed such different behavior in the BLI experiments (Suppl. Figure 5) suggested that the mechanisms by which the two lipids act on PADI4 could be slightly different. At the moment, we cannot rule out that some of these processes inferred by fluorescence experiments were also captured by the two-exponential behavior of the sensorgrams (Figure 2A). In any case, the final conformation of the protein, once bound to the lipid membrane, seems to be similar to that in isolation, at least around its tryptophan residues.

Although we have proved unambiguously the binding between PADI4 and lipids of different sizes, with distinct alkyl chains and different charges, we do not know the exact mechanism by which it occurs neither the exact function of such binding. We speculate that PADI4 could act as a cargo of lipids to satisfy the high demands of these macromolecules during cancer growth, as it has been suggested in some types of aggressive GBM [52]. However, since the origin of the dimeric nature of PADI4 proteins is not well understood, lipids could act as well as anchoring points to the plasma membrane by one of the monomers of the homodimer, whereas the other protomer is still capable of carrying out its enzymatic function. Nevertheless, the binding to the anchoring point would be very weak, as suggested by the apparent disso-

Figure 7. PADI4 binding to phosphatidylserine (PS) *in cellulo* as monitored by PLAs. (A) PLAs of PADI4 with PS reveal the interaction between the protein and the lipid in cancer cell lines (left side panel, HGUE-GB-42 and SW480) and non-cancer cell lines (right side panel, HEK-293 and MCR5). Red fluorescence dots indicate PLA-positive signals representing PADI4/PS interactions. Blue fluorescence dots correspond to DAPI staining of the nuclei. MERGE images show the overlay of PLA (red) and DAPI (blue) signals. (B) Inhibition of the formation of the PADI4/PS complex by the presence of GSK484 *in cellulo* was performed in the HGUE-GB-42 cell line. After 1, 3, and 6 h treatment with 20 μM of GSK484, a decrease in the red signal, which pinpoints to PS-PADI4 interactions, was observed. Notably, the absence of red dots at 6 h implies the complete abolition of detectable interaction. A representative experiment of PLA for each condition is shown (n = 5). Scale bar: 20 μm. (C) The PLA dots of a representative experiment with GSK484 treatment were quantified (n = 5). The Fiji software was used to count the number of red dots. Data represent mean ± standard error of the mean and Student's 2-tailed unpaired *t*-test was used. Asterisks indicate the statistical significance of the results **p < 0.001; *****p < 0.0001. PS-PADI4 interactions (red dots); nuclei (blue, labeled with DAPI). Scale bar: 20 μm.

ciation constants measured by BLI (Figures 2A, B). The presence of the dimeric nature of PADI4 and its interaction with lipids could also explain the inflammatory response where PADI4 intervenes. Neutrophils play an essential role in innate immunity, since they are the first cells recruited to the infection site [53]. Neutrophils can trap and kill various protozoal, fungal and bacterial pathogens by the formation of chromatin structures, known as neutrophil extracellular traps (NETs) [53]. These NETs are generated by activated neutrophils, upon stimulation with inflammatory stimuli-related molecular species like lipopolysaccharides (LPSs), which are at the external membranes of many bacteria and are formed by fatty acids and disaccharides. PADI4 is essential for NET-mediated antibacterial function by citrullinating histones and chemokines [54–56]. Based on our results in this work, we could further hypothesize that PADI4 might be anchored by one of the monomers to some of the lipids that form the LPSs, while the other monomer could be involved in the citrullination of some of the proteins required in NET formation. However, this should be further validated with specific assays to depict the exact mechanism.

Recently, in cross-resistant melanoma cells, genes involved in the synthesis of prostaglandin lipids have been found to be expressed at higher levels than in therapy-response cells [57]. On the other hand, the expression of genes involved in the response to type I interferons is much lower than that in cross-resistant cells [57]. Then, as a third suggestion, we hypothesize that PADI4 could be also involved in the regulation of these other types of lipid species, modulating the response of the cells in different cancers. However, at this stage, we do not favor the possibility that *in cellulo* PADI4 could de-lipidate the membrane, as from the results *in vitro* (Figure 1), PADI4 seems to cause rather the opposite: an association of the LUVs.

PADI proteins requires calcium for catalysis, and the sequential binding of the calcium ions yields to conformational rearrangements in residues forming the active site cleft or close to it [58]. However, the Ca²+ concentrations required for such activation in vitro (larger than 1 mM) [58] are much larger than the intracellular physiological concentrations (\sim 100 nM) [59,60]. Then, under those physiological conditions the binding of PADI4 to lipids would act as mechanism of activation to decrease the amount of Ca²+ required at intracellular level.

Finally, we also hypothesize that lipids could act as natural inhibitors of PADI4 function or of the interactions with some of its molecular partners, which would have a wide range of biological implications, and open the way to several novel therapeutic possibilities. As an example, it has been recently suggested that blood lipid markers appearing in excess during the treatment of docetaxel, a drug for treatment of prostate cancer patients, could be used as markers of

resistance to such drug [61]. We hypothesize that the presence of an excess of several kinds of lipids concomitantly to an increase of the expression levels of PADI4 could be a defense mechanism to modulate, by binding to the active site, the excess of over-expressed enzyme, and then, of citrullinated proteins, during the progress of some maladies.

Conclusion

We have shown for the first time the interaction of the enzyme PADI4 with lipids, occurring at the active site of this protein, as such interaction is hampered in cellulo by the inhibitor of PADI4 and it is also modeled by in silico results. We hypothesized that such interaction could have wide applications in clinical studies, as other lipids have been detected in blood samples and can be used as clinical markers (e.g., of tumor onset or progression) less invasive than biopsies, or markers of therapy responses. In particular, the interaction here reported of PADI4 with several kinds of lipids (and especially with PS) suggests that they could be used in a less invasive early detection of some types of cancers, where PADI4 could intervene. Therefore, this work opens new directions for studying the mechanism underlying tumorigenesis by assessing the relevance of this protein-lipid interaction. Moreover, the differential distribution of the PADI4/PS complexes evidenced between cancer and non-cancer cells opens the venue for developing treatments based on this interaction, while shedding more light on the different mechanism that takes place under pathological conditions as compared with healthy cells.

Materials and Methods

Materials

Imidazole, Trizma base and acid, DNase, glycerol, $N-\alpha$ -Benzoyl-L-arginine ethyl (BAEE), L-citrulline, 3-hydroxyimino 2-butanone (diacetyl monoxime), thiosemicarbazide. dithiothreitol (DTT), SO₄H₂ (96–98%), PO₄H₃ (85%), $NH_4Fe(SO_4)_2\cdot 12$ H_2O , NaCl, antipyrine, SIGMAFAST protease tablets, NaCl, Ni2+-resin, DAPI (4',6-diamidino-2-phenylindole) and ultrapure dioxane were from Sigma (Madrid, Spain). Kanamycin and isopropyl-β-D-1thiogalactopyranoside were obtained from Apollo Scientific (Stockport, UK). Dialysis tubing with a molecular weight cut-off of 3500 Da, Triton X-100, (tris(2-carboxyethyl)phosphine) and the SDS protein marker (PAGEmark Tricolor) were from VWR (Barcelona, Spain). Amicon centrifugal devices with a molecular weight cut-off of 30 kDa were from Millipore (Barcelona, Spain).

The lipids (Suppl. Figure 9) POPC, POPA, L- α phosphatidylcholine from egg chicken (ePC) and L- α -phosphatidylserine from brain porcine (bPS) were from Avanti Polar Lipids (Alabaster, AL, USA). The zwitterionic ePC and anionic bPS are glycerophospholipids, purified from the egg and the brain, respectively. They are formed by a scrambled mixture of different fatty acid chains with the same headgroup: PC or PS, respectively. On the other hand, POPC and POPA are also zwitterionic and anionic lipids, respectively, containing PC or PA as the corresponding head group, but they are formed by a single, unique fatty acid chain: 1-palmitoyl-2-oleoyl acid. The mobility, rigidity and size of these fatty acid chains are responsible of bilayer fluidity and bending properties of the membranes [62], affecting several associated molecular properties and biological processes [63.64].

The rest of the materials was of analytical grade. Water was deionized and purified on a Millipore system.

Protein expression and purification

The dimeric protein PADI4 (with 663 residues *per* monomer) was purified as previously described [21]. Protein concentration was determined by UV absorbance, employing an extinction coefficient at 280 nm estimated from the 10 tryptophans and 13 tyrosines *per* monomer [65].

Cell lines

Isolation of the primary human GBM cell line HGUE-GB-42 was performed from surgical washes, as reported previously [46]. Colorectal cancer (SW-480) cell line was donated by Instituto Municipal de Investigaciones Médicas (IMIM. Barcelona, Spain) [66]. The SW-480 cell line was cultured in Dulbecco's Modified Eagle's Medium: High Glucose (DEMEM-HG) (Biowest, MO, USA). GBM cells were cultured in Dulbecco's Modified Eagle's Medium: Nutrient Mixture F-12 (DMEM F-12) (Biowest, MO, USA). Both mediums were supplemented with 10% (v/v) heat-inactivated fetal bovine serum (FBS) (Capricorn Scientific, Ebsdorfergrund, Germany) and 1% (v/v) penicillin/streptomycin mixture (Biowest, MO, USA). Cells were incubated at 37 °C in a humidified 5% CO2 atmosphere as previously described [67]. Human fetal lung fibroblast cells, MRC-5 (catalog number 05072101), were purchased from Sigma-Aldrich (Madrid, Spain). MRC-5 cells were cultured in Minimum Essential Media (MEM) (Biowest, MO, USA) enriched with 10% FBS, 1% (v/v) penicillin/streptomycin mixture, and 2 mM L-glutamine. Cell cultures were incubated at 37°C in a humidified 5% CO₂ atmosphere. HEK-293, a human embryonic kidney cell line (and therefore, a non-cancerous cell line), was also cultured in the same way as the MRC-5 cells.

Immunofluorescence (IF)

An amount of 35,000 cells of HGUE-GB-42, HEK-293. SW-480, or MRC-5 were seeded into 24-well plates on coverslips. After 24 h, they were fixed with paraformaldehyde at 4% concentration and blocked with fetal bovine serum/phosphate buffered saline (FBS/PBS) (1×) (50 µL FBS/1 mL PBS). Next. cells were treated with 50 mM NH₄Cl (3 times for 5 min each cycle) at 4 °C followed by washes of phosphate buffer containing 0.1% Triton. Cells were blocked in the FBS/PBS solution for 1 h at 4 °C. Then, the cells were anti-PADI4 (1:100, incubated with Invitrogen, Barcelona, Spain) and anti-PS (1:100, mouse; Sigma, Barcelona, Spain) antibodies at 25 °C. After washing out the first antibody, cells were incubated with Alexa Fluor 568-labeled antimouse (1:500) and Alexa Fluor 488-labeled antirabbit (1:500) secondary antibodies (Invitrogen, Barcelona, Spain); the DAPI reagent was used to stain the nucleus. Coverslips were mounted in Prolong™ Gold Anti-fade Reagent (Invitrogen, Barcelona, Spain) and analyzed using a confocal microscope LSM900 with Airyscan 2 (Carl Zeiss, Oberkochen, Germany) at 64× magnification.

Proximity ligation assay (PLA)

An amount of 35,000 cells of HGUE-GB-42, HEK-293, SW-480 or MRC-5 cell lines were seeded in 24-well plates on coverslips. After 24 h, cells were washed in PBS $(1\times)$, fixed with paraformaldehyde 4%, washed again, permeabilized in PBS $(1\times)$ with 0.2% Triton X-100, and blocked with blocking solution for 1 h at 37 °C before immune-staining with Duo-link by using PLA Technology (Merck, Madrid, Spain), following the manufacturer's Anti-PS and anti-PADI4 protocol. antibodies were used. Then, slides processed for in situ PLA by using sequentially the Duolink In Situ PLA Probe Anti-Mouse MINUS, Duolink In Situ PLA Probe Anti-Rabbit PLUS, and Duolink In Situ Detection Reagents Red (Merck, Madrid, Spain). In these experiments, red fluorescence spots correspond to the PLA-positive signal, and they indicate that the two proteins are bound, forming a protein complex, whereas the blue fluorescence signals correspond to nuclei (DAPI staining). Both negative and positive control experiments were performed, the former by omitting one of the primary antibodies. As in the IF experiments, image acquisition was carried out by using a confocal microscope LSM900 with Airyscan 2 (Carl Zeiss, Oberkochen, Germany) at 64× magnification.

PLA statistical analysis

To evaluate the normal distribution of the data, the Shapiro-Wilk statistical test was used; the Student's *t*-test was used to analyze the

association between variables. Differences were statistically significant with a *p*-value <0.05. Statistical analysis was performed with GraphPad Prism v7.0a software (GraphPad Software Inc., San Diego CA, USA).

Lipid vesicle and sample preparation

Lipid vesicles were prepared by dissolving the required amount of lipid in chloroform/methanol (2:1 v/v), and drying, first under a gaseous nitrogen stream and then under vacuum for 3 h, to remove all traces of organic solvents. The thin lipid layer formed was resuspended in 20 mM Tris–HCl, 5 mM TCEP, 150 mM NaCl, 5% glycerol (pH 7) buffer while being vortexed. The resulting multilamellar liposome suspensions were extruded through 100 nm polycarbonate filters (Nucleopore, Cambridge, MA) to obtain large unilamellar vesicles (LUVs).

Static light scattering of LUVs

Measurements were done in a Cary Varian (Agilent, Madrid, Spain) spectrofluorimeter (with excitation, λ_{ex} , and emission, λ_{em} , at wavelengths of 500 nm). A 1 mM LUV solution was placed in a quartz cuvette of 10 mm light path (1.5 mL), and sequential additions of PADI4, from a stock solution of 70 µM, were made every 5 min. Final sample dilution was always lower than 6.5% and. in any case, its effect on data obtained from the measurements was corrected. All experiments were performed with samples thermostated at 25 $^{\circ}$ C by using a Peltier system, and under magnetic stirring. In these experiments, POPC or POPA were used to ensure that the heterogeneity of the fatty acid chain in the tested lipids did not affect the binding to PADI4.

Anisotropy fluorescence measurements

The anisotropy fluorescence measurements were performed in a PicoQuant F300 (PicoQuant, Berlin, Germany) spectrofluorometer. A solution containing 1 µM PADI4 was placed in a quartz cuvette of 5 mm light path, and sequential additions of LUVs from a 10 mM stock solution were made, with 5 min of equilibration time before performing the measurements. For comparison, a blank sample without protein was prepared, treated and measured in the same way. Final dilution of the corresponding solutions was always less than 6.5%. All experiments were performed with samples thermostated at 25 °C by using a Peltier system. Measurements for each lipid concentration were carried out in duplicate, and in all cases variations between the measurements were lower than 5%. Steady-state anisotropy was measured at 340 nm by using an excitation wavelength of 300 nm and calculated as:

$$\langle r \rangle = (I_{VV} - GI_{VH})/(I_{VV} + 2GI_{VH}),$$
 (1)

where $l_{\rm VV}$ and $l_{\rm VH}$ are the fluorescence intensities (blank subtracted) of the vertically and horizontally polarized emission, respectively, when the sample is excited with vertically polarized light. The *G*-factor corresponds to the instrument correction factor ($G = l_{\rm VH}/l_{\rm HH}$). Data are the average of ten measurements.

In the anisotropy measurements, we used LUVs formed by: (i) ePC, which is a zwitterionic lipid, to test for the absence of a net charge in the lipid species binding to PADI4; and (ii) a mixture of ePC (75 w/w) and bPS (25 w/w), where the percentage of the latter is higher than that found in membranes in the cell, to find out the influence of a lipid mixture in the binding.

Biolayer interferometry (BLI)

In the BLI experiment, we used the same LUVs as those in the anisotropy measurements.

Experimental design of the BLI experiments in the absence of GSK484. The association (k_{on}) and dissociation (k_{off}) rate constants of the binding of the lipids to PADI4 were determined by using a BLItz system (ForteBio, Pall, Barcelona, Spain) [68]. The buffer used in the experiments was that recommended by the manufacturer. As PADI4 had a His-tag, it was immobilized on His-tag biosensors (Forte Bio) at a concentration of 0.57 µM. Experiments were carried out at 25 °C, and points were collected every 0.2 s. The general schemes of the protein/lipid association/dissociation reactions in the BLItz system were: 30 s of acquisition of the initial baseline with the 10× kinetics buffer; 120 s of loading PADI4 into the biosensor; 30 s of baseline acquisition with the 10× kinetics buffer; 120 s of association of the LUV to the biosensor (which had been previously loaded with PADI4); and 120 s of dissociation of the LUV from the biosensor with the 10× kinetics buffer.

Experimental design of the BLI experiments in the presence of GSK484. The association (k_{on}) and dissociation (k_{off}) rate constants of the binding of the lipids to PADI4 in the presence of 110 μM of GSK484 were determined by using a BLItz system (ForteBio, Pall, Barcelona, Spain) [68]. The buffer used in the experiments was that recommended by the manufacturer. As PADI4 had a Histag, it was immobilized on His-tag biosensors (ForteBio) at a concentration of 0.57 μM. Experiments were carried out at 25 °C, and points were collected every 0.2 s. The general schemes of the protein/ lipid association/dissociation reactions in the BLItz system were similar to those described above, except for the presence of the inhibitor at every step: 30 s of acquisition of the initial baseline with the 10 \times kinetics buffer in the presence of 110 μ M of GSK484; 120 s of loading PADI4 (at a concentration of 0.57 µM) into the biosensor in the presence of 110 µM of GSK484; 30 s of baseline acquisition with the 10× kinetics buffer in the presence of 110 μM of GSK484; 120 s of association of the LUV in the presence of 110 μM of GSK484 to the biosensor (which had been previously loaded with the PADI4/GSK484 complex); and 120 s of dissociation of the LUV from the biosensor with the 10× kinetics buffer in the presence of 110 μM of GSK484.

Fitting of the BLI sensorgrams. Fittings of the sensorgrams either in the absence or in the presence of GSK484, when it was possible, was carried out by using KaleidaGraph (Synergy software, Reading, PA, USA) [69]. The interferometry response during the association step, R(t) (measured in response units, RU), and the binding rate, dR(t)/dt, can be used to evaluate the kinetics of the formation of the PADI4/LUV complex, according to:

$$\frac{dR(t)}{dt} = k_{on}[lipid](R_{max} - R(t)) - k_{off}R(t), \tag{2}$$

where $R_{\rm max}$ is proportional to the total concentration of biosensor-bound PADI4; and [lipid] represents the corresponding concentration of lipids in the form of LUVs.

In Eq. (2), R(t) is given by:

$$R(t) = R_{eq} - R_{eq} e^{(-k_{obs} (t - t_0))}$$
(3)

where $R_{\rm eq}$ is the steady-state (or equilibrium) response obtained at virtually infinite time when ${\rm d}R(t)/{\rm d}t=0$, and $t_0=180$ s is the time at which the association step between biosensorimmobilized PADI4 and LUV in the solution started. As we observed a slope of the signal at the largest sensorgram acquisition times, we fitted the R(t) experimentally obtained under most of the conditions (see Section 'Discussion') by using two exponential contributions:

$$R(t) = R_{eq} - R_{eq} e^{(-k_{obs} (t-t_0))} - R'_{eq} e^{(-k_{obs} (t-t_0))} - R''_{eq} (t - t_0)$$

$$(4)$$

We tried to fit the sensorgrams to a single exponential equation, but F-test analyses indicated that the fitting was better with two exponential contributions. This finding suggested that the binding process was not two-state. The difference between the two $k_{\rm obs}$ values, in the comparison between ePC and bPS, was an order of magnitude. We carried out the pseudo-first order plots with the largest $k_{\rm obs}$ value measured, where its value is given by:

$$k_{obs} = k_{on} [lipid] + k_{off}$$
 (5)

The dissociation process of the LUV from PADI4 attached to the biosensor was always fitted by using a single exponential, with R(t) given by:

$$R(t) = R_1 e^{(-k_{\text{off}}(t-t_0))} - R_2(t-t_0)$$
 (6)

where $t_0 = 300$ s is the time at which the dissociation of lipid from the biosensor-bound PADI4 started in

our experiments, and R_1 is the response level when dissociation started.

For the experiments in the presence of 110 μ M of GSK484, the sensorgrams of the association step for ePC or ePC/bPS could not be fitted to the Eq. (4) above (Suppl. Figure 5). Furthermore, for the dissociation step in the presence of 110 μ M of GSK484 with ePC/bPS, data could not be fitted to Eq. (5) above.

Bioinformatic analysis of putative lipid-binding regions of PADI4

A bioinformatic scan of the sequence of PADI4 was performed, to explore its lipid binding properties based on a hydropathy analysis of its amino acid composition. The analysis was performed by using the software tool MPEx, version 3.3.1 [70]. This algorithm is modeled in analogy to the widely used hydrophobicity plot of Kyte and Doolittle [71], by using a sliding-window evaluation of 7-11 protein residues - an even number centered on each consecutive amino acid along the sequence. In particular, MPEx analysis is based upon the experiment-based hydropathy scale determined by White and Wimley [43], which measures the free energy of transfer from water to a bilayer hydrocarbon core of a protein segment. Therefore, this scale identifies the regions of a protein chain most likely to be involved in the association with membranes.

Molecular docking of the lipids on the PADI4 surface

Molecular docking of our lipids to PADI4 was performed by using DiffDock, one of the most promising algorithms currently developed [44], which consists in a novel generative model that mimics a diffusion process over the manifold of ligand poses. The number of inference steps varied between 20 and 40, and the number of samples was 40. The confidence score obtained (c ≈ -1.5) indicates adequate reliability of the binding conformations obtained, but does not predict their binding affinity. Therefore, we also used molecular mechanics with generalized Born surface area (MM/GBSA) solvation [72], as implemented in the web server fastDRH [73], to analyze the most favorable lipid conformation obtained in each simulation.

Small overlaps between PADI4 and the docking poses of the lipids were preliminarily relaxed by performing an energy minimization with 100 steps of steepest descent algorithm, with a step size of 0.02 Å. In the MM/GBSA calculations, the force fields used were Amber ff19SB [74] and GAFF2 [75] for the protein and the lipids, respectively, in combination with the water model OPC [76]. To improve the accuracy, the only modification with respect to the default input parameters was that interactions between the protein and lipids were

not truncated (i.e., threshold radius \geq 50 Å) beyond a cut-off. The binding energy was obtained by averaging the best three MM/GBSA rescoring procedures available in fastDRH [73], referred to as GB1, GB2 and GB5.

Determination of citrullination by a colorimetric assay

A photometric method used for the determination of L-citrulline was applied to investigate whether PADI4 was capable of citrullinating BAEE in the presence of each lipid. This method is based in the reaction of citrulline with oxymes, such as diacetyl monoxime, in strong acids in the presence of thiosemicarbazide. The protocol to prepare the color developed reagent (COLDER) has been described elsewhere [41] and applied to detect the enzymatic activity of PADI4 [77,78]. We also used to monitor the citrullination the modification of the above colored reagent reaction, with the presence of oxime and antipyrine in strong acids, but without the thiosemicarbazide [42]. In the COLDER reaction, when using thiosemicarbazide, the color of the product (red-pink) is due to the reaction between the ureido group (present in the citrulline) and the monoxime, in the presence of thiosemicarbazide and Fe(III) at highly acidic pH.

In the case of using antipyrine (but not thiosemicarbazide), the oxime and the ureido react to yield an imidazolone, which in turn, reacts with the antipyrine through its enamine group [79]. This reaction yields a yellow colored product.

All absorption spectra were recorded between 400 and 600 nm on an UV–Visible spectrophotometer UV-1603 by Shimadzu (Kyoto, Japan). All spectra were acquired at room temperature. Water was used as a reference for a blank subtraction for all the analyzed samples.

We used the same procedure described elsewhere, including the same controls [78]. All the reactions were made in duplicate for each of the two colored reagents. We also used as control the reaction of citrullination of BAEE in the presence of saturating conditions of GSK484 (110 µM). The reaction buffer contained 100 mM Tris (pH 7.6), 50 mM NaCl, 2 mM DTT and 10 mM CaCl₂ up to a final volume of 500 µL. We added PADI4 from a stock solution to the tubes containing the reaction buffer to yield a final concentration of 0.75 µM (in protomer units), except for the blank solution. The resulting solutions were incubated for 25 min at 37 °C in an Innova 4000 new Brunswick scientific incubator (Thermofisher, Madrid, Spain) with a 190 rpm shaking. After such period of time, we added BAEE from a stock solution to vield a final concentration of 100 µM. For the control reaction with L-citrulline, the corresponding volume from a stock solution of L-citrulline was added to the control tube, to yield a final concentration of 100 µM. Samples were incubated at 37 °C for 25 min in the same shaker with agitation. Reactions were

quenched by flash freezing in liquid nitrogen. For color development, 2 mL of freshly prepared COLDER solution was added to the quenched reaction, vortexed to ensure complete mixing, and incubated for 15 min at 95 °C; the same amount of reagent containing antipyrine was added to the other tubes in parallel. After cooling at room temperature, the samples were transferred into 1 mL-quartz cuvettes to perform the measurements in the spectrophotometer.

Resource availability

All the materials are available upon reasonable request from the corresponding authors.

CRediT authorship contribution statement

Salomé Araujo-Abad: Writing – review & editing. Writing – original draft, Methodology, Investigation, Funding acquisition, Formal analysis. Conceptualization. Borja García-Peñarrubia: & editing, Writina review Methodology. Investigation, Formal analysis. A.Marcela Giudici: Writing - review & editing, Writing original draft, Methodology, Investigation, Formal analysis. José L. Neira: Writing - review & editing, Writing original draft, Proiect administration. Methodology, Investigation, Funding acquisition, Formal analysis. Conceptualization. Bruno Rizzuti: Writing review & editing, Writing - original draft, Methodology, Investigation, Formal analysis, Conceptualization. Camino de Juan Romero: Writing - review & editing, Writing - original draft, Project administration, Methodology, Investigation, Funding acquisition, Formal analysis. Conceptualization. José A. Poveda: Writing review & editing, Writing - original draft, Methodology, Investigation, Formal analysis, Conceptualization.

DATA AVAILABILITY

Data will be made available on request.

DECLARATION OF COMPETING INTEREST

The authors declare that they have no known competing financial interests or personal relationships that could have appeared to influence the work reported in this paper.

Acknowledgements and Funding

This research was funded by Instituto de Salud Carlos III (ISCIII) and cofounded by European Social Fund (ERDF/ESF, "Investing in your

future") [MS19/00095 and PI22/00824 to CdJ]; and Comunidad Valenciana [CIAICO 2021/0135 to CdJ, JAP and JLN], and by European Union [EXPLORA GA no. 101181841 to JLN]. SAA was supported by Universidad de Las Américas funding [525.A.XV.24]. BR acknowledges the use of the distributed laboratory of molecular modeling funded by Next Generation EU program, Italian PNNR, Mission 4, Component 2, Investment 1.5, "Innovation Ecosystems" project Tech4You, "Technologies for Climate Change Adaptation and Quality of Life Improvement" (CUP B83C22003980006), Spoke 3. The funders had no role in the study design, data collection and analysis, decision to publish, or preparation of the manuscript.

We thank the three anonymous reviewers for helpful suggestions, corrections and discussions. We thank Prof. Georg E. Schulz for handling the manuscript.

Appendix A. Supplementary material

Supplementary material to this article can be found online at https://doi.org/10.1016/j.jmb.2025. 169297.

Received 17 April 2025; Accepted 11 June 2025; Available online 16 June 2025

Keywords:

protein-lipid interactions; citrullinating enzyme; proximity ligation assay; molecular docking; immunofluorescence

Abbreviations:

BLI, biolayer interferometry; COAD, colon cancer; COLDER, color developing reagent; bPS, brain PS; DTT, dithiothreitol; FBS, fetal bovine serum; FRET, Förster resonance energy transfer; GBM, glioblastoma; IF, immunofluorescence; LPS, lipopolysaccharide; LUV, large unilamellar vesicles; MM/GBSA, molecular mechanics with generalized Born surface area; NET, neutrophil extracellular trap; NR, nuclear reticulum; PA, phosphatidic acid; PC, phosphatidylcholine; PBS, phosphate buffer saline; ePC, egg phopshatidylcoline; PAAD, pancreatic adenocarcinoma; PLA, proximity ligation assay; POPA, 1-palmitoyl-2-oleoyl-sn-glycero-3-phosphate (sodium salt); POPC, 1-palmitoyl-2-oleoyl-sn-glycero-3-phosphocholine; PS, phosphatidylserine

References

[1]. Molendijk, J., Robinson, H., Djuric, Z., Hill, M.M., (2020). Lipid mechanisms in hallmarks of cancer. *Mol. Omics* 16, 6–18. https://doi.org/10.1039/C9MO00128J.

- [2]. Saito, R. de F., Andrade, L.N. de S., Bustos, S.O., Chammas, R., (2022). Phosphatidylcholine-derived lipid mediators: the crosstalk between cancer cells and immune cells. *Front. Immunol.* 13, 768606. https://doi. org/10.3389/FIMMU.2022.768606/BIBTEX.
- [3]. Foster, D.A., Xu, L., (2003). Phospholipase D in cell proliferation and cancer. Mol. Cancer Res. 1, 789–800.
- [4]. Bruntz, R.C., Lindsley, C.W., Brown, H.A., (2014). Phospholipase D signaling pathways and phosphatidic acid as therapeutic targets in cancer. *Pharmacol. Rev.* 66, 1033–1079. https://doi.org/10.1124/PR.114.009217.
- [5]. Kay, J.G., Grinstein, S., (2011). Sensing phosphatidylserine in cellular membranes. Sensors (Basel) 11, 1744–1755. https://doi.org/10.3390/ S110201744.
- [6]. Deserno, M., (2024). Biomembranes balance many types of leaflet asymmetries. *Curr. Opin. Struct. Biol.* 87 https:// doi.org/10.1016/J.SBI.2024.102832.
- [7]. Bevers, E.M., Comfurius, P., Zwaal, R.F.A., (1996). Regulatory mechanisms in maintenance and modulation of transmembrane lipid asymmetry: pathophysiological implications. *Lupus* 5, 480–487. https://doi.org/10.1177/ 096120339600500531.
- [8]. Davis, H.W., Hussain, N., Qi, X., (2016). Detection of cancer cells using SapC-DOPS nanovesicles. Mol. Cancer 15, 1–7. https://doi.org/10.1186/S12943-016-0519-1/FIGURES/4.
- [9]. Huang, X., Bennett, M., Thorpe, P.E., (2005). A monoclonal antibody that binds anionic phospholipids on tumor blood vessels enhances the antitumor effect of docetaxel on human breast tumors in mice. *Cancer Res.* 65, 4408–4416. https://doi.org/10.1158/0008-5472.CAN-05-0031.
- [10]. Budhu, S., Giese, R., Gupta, A., Fitzgerald, K., Zappasodi, R., Schad, S., Hirschhorn, D., Campesato, L.F., De Henau, O., Gigoux, M., Liu, C., Mazo, G., Deng, L., Barker, C.A., Wolchok, J.D., Merghoub, T., (2021). Targeting phosphatidylserine enhances the anti-tumor response to tumor-directed radiation therapy in a preclinical model of melanoma. *Cell Rep.* 34 https://doi.org/10.1016/J.CELREP.2020.108620.
- [11]. N'Guessan, K.F., Patel, P.H., Qi, X., (2020). SapC-DOPS – a phosphatidylserine-targeted nanovesicle for selective cancer therapy. *Cell Commun. Signal* 18 https://doi.org/ 10.1186/S12964-019-0476-6.
- [12]. Sarmento, M.J., Llorente, A., Petan, T., Khnykin, D., Popa, I., Nikolac Perkovic, M., Konjevod, M., Jaganjac, M., (2023). The expanding organelle lipidomes: current knowledge and challenges. *Cell Mol. Life Sci* 80 https:// doi.org/10.1007/S00018-023-04889-3.
- [13]. Niu, Y., Pemberton, J.G., Kim, Y.J., Balla, T., (2024). Phosphatidylserine enrichment in the nuclear membrane regulates key enzymes of phosphatidylcholine synthesis. *EMBO J.* 43, 3414–3449. https://doi.org/10.1038/S44318-024-00151-Z.
- [14]. Corn, K.C., Windham, M.A., Rafat, M., (2020). Lipids in the tumor microenvironment: from cancer progression to treatment. *Prog. Lipid Res.* 80 https://doi.org/10.1016/ j.plipres.2020.101055.
- [15]. Szlasa, W., Zendran, I., Zalesińska, A., Tarek, M., Kulbacka, J., (2020). Lipid composition of the cancer cell membrane. J. Bioenerg. Biomembr. 52, 321–342. https://doi.org/10.1007/S10863-020-09846-4.

- [16]. Fowle-Grider, R., Rowles, J.L., Shen, I., Wang, Y., Schwaiger-Haber, M., Dunham, A.J., Jayachandran, K., Inkman, M., Zahner, M., Naser, F.J., Jackstadt, M.M., Spalding, J.L., Chiang, S., McCommis, K.S., Dolle, R.E., Kramer, E.T., Zimmerman, S.M., Souroullas, G.P., Finck, B.N., Shriver, L.P., Kaufman, C.K., Schwarz, J.K., Zhang, J., Patti, G.J., (2024). Dietary fructose enhances tumour growth indirectly via interorgan lipid transfer. *Nature* 636 https://doi.org/10.1038/S41586-024-08258-3.
- [17]. Yuzhalin, A.E., (2019). Citrullination in cancer. Cancer Res. 79, 1274–1284. https://doi.org/10.1158/0008-5472. CAN-18-2797.
- [18]. Gudmann, N.S., Hansen, N.U.B., Jensen, A.C.B., Karsdal, M.A., Siebuhr, A.S., (2015). Biological relevance of citrullinations: diagnostic, prognostic and therapeutic options. *Autoimmunity* 48, 73–79. https://doi. org/10.3109/08916934.2014.962024.
- [19]. Ishigami, A., Maruyama, N., (2010). Importance of research on peptidylarginine deiminase and citrullinated proteins in age-related disease. *Geriatr. Gerontol. Int.* 10, S53–S58. https://doi.org/10.1111/J.1447-0594.2010.00593.X.
- [20]. György, B., Tóth, E., Tarcsa, E., Falus, A., Buzás, E.I., (2006). Citrullination: a posttranslational modification in health and disease. *Int. J. Biochem. Cell Biol.* 38, 1662– 1677. https://doi.org/10.1016/J.BIOCEL.2006.03.008.
- [21]. Neira, J.L., Araujo-Abad, S., Cámara-Artigas, A., Rizzuti, B., Abian, O., Giudici, A.M., Velazquez-Campoy, A., de Juan Romero, C., (2022). Biochemical and biophysical characterization of PADI4 supports its involvement in cancer. *Arch. Biochem. Biophys.* 717, 109125. https://doi.org/10.1016/J.ABB.2022.109125.
- [22]. Ying, S., Dong, S., Kawada, A., Kojima, T., Chavanas, S., Méchin, M.C., Adoue, V., Serre, G., Simon, M., Takahara, H., (2009). Transcriptional regulation of peptidylarginine deiminase expression in human keratinocytes. *J. Dermatol. Sci.* 53, 2–9. https://doi.org/10.1016/J. JDERMSCI.2008.09.009.
- [23]. Slade, D.J., Horibata, S., Coonrod, S.A., Thompson, P.R., (2014). A novel role for protein arginine deiminase 4 in pluripotency: the emerging role of citrullinated histone H1 in cellular programming. *Bioessays* 36, 736–740. https:// doi.org/10.1002/BIES.201400057.
- [24]. Witalison, E., Thompson, P., Hofseth, L., (2015). Protein arginine deiminases and associated citrullination: physiological functions and diseases associated with dysregulation. *Curr. Drug Targets* 16, 700–710. https:// doi.org/10.2174/1389450116666150202160954.
- [25]. Wang, Y., Chen, R., Gan, Y., Ying, S., (2021). The roles of PAD2- and PAD4-mediated protein citrullination catalysis in cancers. *Int. J. Cancer* 148, 267–276. https://doi.org/10.1002/IJC.33205.
- [26]. Yang, C., Dong, Z.Z., Zhang, J., Teng, D., Luo, X., Li, D., Zhou, Y., (2021). Peptidylarginine deiminases 4 as a promising target in drug discovery. Eur. J. Med. Chem. 226 https://doi.org/10.1016/J.EJMECH.2021.113840.
- [27]. Hung, H.C., Lin, C.Y., Liao, Y.F., Hsu, P.C., Tsay, G.J., Liu, G.Y., (2007). The functional haplotype of peptidylarginine deiminase IV (S55G, A82V and A112G) associated with susceptibility to rheumatoid arthritis dominates apoptosis of acute T leukemia Jurkat cells. *Apoptosis* 12, 475–487. https://doi.org/10.1007/S10495-006-0005-0.

- [28]. Li, P., Yao, H., Zhang, Z., Li, M., Luo, Y., Thompson, P.R., Gilmour, D.S., Wang, Y., (2008). Regulation of p53 target gene expression by peptidylarginine deiminase 4. Mol. Cell Biol. 28, 4758. https://doi.org/10.1128/MCB.01747-07.
- [29]. Li, P., Wang, D., Yao, H., Doret, P., Hao, G., Shen, Q., Qiu, H., Zhang, X., Wang, Y., Chen, G., Wang, Y., (2010). Coordination of PAD4 and HDAC2 in the regulation of p53-target gene expression. *Oncogene* 29, 3153–3162. https://doi.org/10.1038/onc.2010.51.
- [30]. Neira, J.L., Rizzuti, B., Abián, O., Araujo-Abad, S., Velázquez-Campoy, A., de Juan Romero, C., (2022). Human enzyme PADI4 binds to the nuclear carrier importin α3. Cells 11 https://doi.org/10.3390/ CELLS11142166.
- [31]. Neira, J.L., Rizzuti, B., Araujo-Abad, S., Abian, O., Fárez-Vidal, M.E., Velazquez-Campoy, A., de Juan Romero, C., (2023). The armadillo-repeat domain of Plakophilin 1 binds to human enzyme PADI4. Biochim. Biophys. Acta Proteins Proteom. 1871 https://doi.org/10.1016/J. BBAPAP.2022.140868.
- [32]. Araujo-Abad, S., Rizzuti, B., Soto-Conde, L., Vidal, M., Abian, O., Velazquez-Campoy, A., Neira, J.L., de Juan Romero, C., (2024). Citrullinating enzyme PADI4 and transcriptional repressor RING1B bind in cancer cells. *Int. J. Biol. Macromol.* 274 https://doi.org/10.1016/J. IJBIOMAC.2024.133163.
- [33]. Araujo-Abad, S., Rizzuti, B., Villamarin-Ortiz, A., Pantoja-Uceda, D., Moreno-Gonzalez, C.M., Abian, O., Velazquez-Campoy, A., Neira, J.L., de Juan Romero, C., (2023). New insights into cancer: MDM2 binds to the citrullinating enzyme PADI4. *Protein Sci.* 32 https://doi.org/10.1002/PRO.4723.
- [34]. Araujo-Abad, S., Fuentes-Baile, M., Rizzuti, B., Bazán, J. F., Villamarin-Ortiz, A., Saceda, M., Fernández, E., Vidal, M., Abian, O., Velazquez-Campoy, A., de Juan Romero, C., Neira, J.L., (2023). The intrinsically disordered, epigenetic factor RYBP binds to the citrullinating enzyme PADI4 in cancer cells. *Int. J. Biol. Macromol.* 246, 125632. https://doi.org/10.1016/J. IJBIOMAC.2023.125632.
- [35]. Araujo-Abad, S., Neira, J.L., Rizzuti, B., García-Morales, P., de Juan Romero, C., Santofimia-Castaño, P., Iovanna, J., (2023). Intrinsically disordered chromatin protein NUPR1 binds to the enzyme PADI4. *J. Mol. Biol.* 435 https://doi.org/10.1016/J.JMB.2023.168033.
- [36]. Zhu, C., Liu, C., Chai, Z., (2023). Role of the PADI family in inflammatory autoimmune diseases and cancers: a systematic review. Front. Immunol. 14 https://doi.org/ 10.3389/FIMMU.2023.1115794.
- [37]. Alghamdi, M., Al Ghamdi, K.A., Khan, R.H., Uversky, V. N., Redwan, E.M., (2019). An interplay of structure and intrinsic disorder in the functionality of peptidylarginine deiminases, a family of key autoimmunity-related enzymes. *Cell. Mol. Life Sci.* 76, 4635–4662. https://doi.org/10.1007/S00018-019-03237-8.
- [38]. Marquette, A., Lorber, B., Bechinger, B., (2010). Reversible liposome association induced by LAH4: a peptide with potent antimicrobial and nucleic acid transfection activities. *Biophys. J.* 98, 2544–2553. https://doi.org/10.1016/J.BPJ.2010.02.042.
- [39]. O'Shannessy, D.J., Winzor, D.J., (1996). Interpretation of deviations from pseudo-first-order kinetic behavior in the characterization of ligand binding by biosensor

- technology. *Anal. Biochem.* **236**, 275–283. https://doi.org/10.1006/ABIO.1996.0167.
- [40]. Barrera, F.N., Poveda, J.A., González-Ros, J.M., Neira, J. L., (2003). Binding of the C-terminal sterile α motif (SAM) domain of human p73 to lipid membranes. *J. Biol. Chem.* 278 https://doi.org/10.1074/jbc.M307846200.
- [41]. Knipp, M., Vašák, M., (2000). A colorimetric 96-well microtiter plate assay for the determination of enzymatically formed citrulline. *Anal. Biochem.* 286, 257–264. https://doi.org/10.1006/ABIO.2000.4805.
- [42]. Sugawara, K., Yoshizawa, Y., Tzeng, S., Epstein, W.L., Fukuyama, K., (1998). Colorimetric determination of citrulline residues in proteins. *Anal. Biochem.* 265, 92– 96. https://doi.org/10.1006/ABIO.1998.2925.
- [43]. White, S.H., Wimley, W.C., (1999). Membrane protein folding and stability: physical principles. *Annu. Rev. Biophys. Biomol. Struct.* 28, 319–365. https://doi.org/ 10.1146/ANNUREV.BIOPHYS.28.1.319.
- [44]. Corso, G., Stärk, H., Jing, B., Barzilay, R., Jaakkola, T., (2022). DiffDock: diffusion steps, twists, and turns for molecular docking. 11th International Conference on Learning Representations, ICLR 2023 (accessed November 20, 2024) https://arxiv.org/abs/2210.01776v2.
- [45]. Isert, C., Atz, K., Schneider, G., (2023). Structure-based drug design with geometric deep learning. *Curr. Opin. Struct. Biol.* **79** https://doi.org/10.1016/J. SBI.2023.102548.
- [46]. Ventero, M.P., Fuentes-Baile, M., Quereda, C., Perez-Valeciano, E., Alenda, C., Garcia-Morales, P., Esposito, D., Dorado, P., Barbera, V.M., Saceda, M., (2019). Radiotherapy resistance acquisition in glioblastoma. Role of SOCS1 and SOCS3. PLoS One 14 https://doi.org/10.1371/JOURNAL.PONE.0212581.
- [47]. Corsetto, P.A., Zava, S., Rizzo, A.M., Colombo, I., (2023). The critical impact of sphingolipid metabolism in breast cancer progression and drug response. *Int. J. Mol. Sci.* 24 https://doi.org/10.3390/IJMS24032107.
- [48]. Tufail, M., Jiang, C.-H., Li, N., (2024). Altered metabolism in cancer: insights into energy pathways and therapeutic targets. *Mol. Cancer* 23, 203. https://doi.org/10.1186/ S12943-024-02119-3.
- [49]. Wang, Q., Zheng, C., Hou, H., Bao, X., Tai, H., Huang, X., Li, Z., Li, Z., Wang, Q., Pan, Q., Wang, L., Zhou, S., Bian, Y., Pan, Q., Gong, A., Xu, M., (2024). Interplay of sphingolipid metabolism in predicting prognosis of GBM patients: towards precision immunotherapy. *J. Cancer* 15, 275–292. https://doi.org/10.7150/JCA.89338.
- [50]. Ran, S., Thorpe, P.E., (2002). Phosphatidylserine is a marker of tumor vasculature and a potential target for cancer imaging and therapy. *Int. J. Radiat. Oncol. Biol. Phys.* 54, 1479–1484. https://doi.org/10.1016/S0360-3016(02)03928-7.
- [51]. Riedl, S., Rinner, B., Asslaber, M., Schaider, H., Walzer, S., Novak, A., Lohner, K., Zweytick, D., (2011). In search of a novel target phosphatidylserine exposed by non-apoptotic tumor cells and metastases of malignancies with poor treatment efficacy. *Biochim. Biophys. Acta* 1808, 2638–2645. https://doi.org/10.1016/J. BBAMEM.2011.07.026.
- [52]. Kloosterman, D.J., Erbani, J., Boon, M., Farber, M., Handgraaf, S.M., Ando-Kuri, M., Sánchez-López, E., Fontein, B., Mertz, M., Nieuwland, M., Liu, N.Q., Forn-Cuni, G., van der Wel, N.N., Grootemaat, A.E., Reinalda, L., van Kasteren, S.I., de Wit, E., Ruffell, B., Snaar-

- Jagalska, E., Petrecca, K., Brandsma, D., Kros, A., Giera, M., Akkari, L., (2024). Macrophage-mediated myelin recycling fuels brain cancer malignancy. *Cell* **187** https://doi.org/10.1016/J.CELL.2024.07.030.
- [53]. Scapini, P., Lapinet-Vera, J.A., Gasperini, S., Calzetti, F., Bazzoni, F., Cassatella, M.A., (2000). The neutrophil as a cellular source of chemokines. *Immunol. Rev.* 177, 195– 203. https://doi.org/10.1034/J.1600-065X.2000.17706.X.
- [54]. Brinkmann, V., Reichard, U., Goosmann, C., Fauler, B., Uhlemann, Y., Weiss, D.S., Weinrauch, Y., Zychlinsky, A., (2004). Neutrophil extracellular traps kill bacteria. *Science* 303, 1532–1535. https://doi.org/10.1126/ SCIENCE.1092385.
- [55]. Li, P., Li, M., Lindberg, M.R., Kennett, M.J., Xiong, N., Wang, Y., (2010). PAD4 is essential for antibacterial innate immunity mediated by neutrophil extracellular traps. J. Exp. Med. 207, 1853–1862. https://doi.org/ 10.1084/JEM.20100239.
- [56]. Moelants, E.A.V., van Damme, J., Proost, P., (2011). Detection and quantification of citrullinated chemokines. PLoS One 6 https://doi.org/10.1371/JOURNAL. PONE.0028976.
- [57]. Elewaut, A., Estivill, G., Bayerl, F., Castillon, L., Novatchkova, M., Pottendorfer, E., Hoffmann-Haas, L., Schönlein, M., Nguyen, T.V., Lauss, M., Andreatta, F., Vulin, M., Krecioch, I., Bayerl, J., Pedde, A.-M., Fabre, N., Holstein, F., Cronin, S.M., Rieser, S., Laniti, D.D., Barras, D., Coukos, G., Quek, C., Bai, X., Muñoz I Ordoño, M., Wiesner, T., Zuber, J., Jönsson, G., Böttcher, J.P., Vanharanta, S., Obenauf, A.C., (2025). Cancer cells impair monocyte-mediated T cell stimulation to evade immunity. Nature 637 https://doi.org/10.1038/S41586-024-08257-4.
- [58]. Arita, K., Hashimoto, H., Shimizu, T., Nakashima, K., Yamada, M., Sato, M., (2004). Structural basis for Ca(2+)induced activation of human PAD4. *Nature Struct. Mol. Biol.* 11, 777–783. https://doi.org/10.1038/NSMB799.
- [59]. Raffaello, A., Mammucari, C., Gherardi, G., Rizzuto, R., (2016). Calcium at the center of cell signaling: interplay between endoplasmic reticulum, mitochondria, and lysosomes. *Trends Biochem. Sci.* 41, 1035–1049. https://doi.org/10.1016/J.TIBS.2016.09.001.
- [60]. Bagur, R., Hajnóczky, G., (2017). Intracellular Ca²⁺ sensing: its role in calcium homeostasis and signaling. Mol. Cell 66, 780–788. https://doi.org/10.1016/J. MOLCEL.2017.05.028.
- [61]. Finnerty, M.C., Leach, F.E., Zakharia, Y., Nepple, K.G., Bartlett, M.G., Henry, M.D., Cummings, B.S., (2024). Identification of blood lipid markers of docetaxel treatment in prostate cancer patients. *Sci. Rep.* 14, 22069. https:// doi.org/10.1038/S41598-024-73074-8.
- [62]. Antonny, B., Vanni, S., Shindou, H., Ferreira, T., (2015). From zero to six double bonds: phospholipid unsaturation and organelle function. *Trends Cell Biol.* 25, 427–436. https://doi.org/10.1016/J.TCB.2015.03.004.
- [63]. Bigay, J., Antonny, B., (2012). Curvature, lipid packing, and electrostatics of membrane organelles: defining cellular territories in determining specificity. *Dev. Cell* 23, 886–895. https://doi.org/10.1016/J. DEVCEL.2012.10.009.
- [64]. Harayama, T., Riezman, H., (2018). Understanding the diversity of membrane lipid composition. *Nature Rev. Mol. Cell Biol.* 19, 281–296. https://doi.org/10.1038/ NRM.2017.138.

- [65]. Gill, S.C., von Hippel, P.H., (1989). Calculation of protein extinction coefficients from amino acid sequence data. *Anal. Biochem.* 182, 319–326. https://doi.org/10.1016/ 0003-2697(89)90602-7.
- [66]. Fuentes-Baile, M., Bello-Gil, D., Pérez-Valenciano, E., Sanz, J.M., García-Morales, P., Maestro, B., Ventero, M. P., Alenda, C., Barberá, V.M., Saceda, M., (2020). CLytA-DAAO, free and immobilized in magnetic nanoparticles, induces cell death in human cancer cells. *Biomolecules* 10 https://doi.org/10.3390/BIOM10020222.
- [67]. Fuentes-Baile, M., Pérez-Valenciano, E., García-Morales, P., Romero, C. de J., Bello-Gil, D., Barberá, V.M., Rodríguez-Lescure, Á., Sanz, J.M., Alenda, C., Saceda, M., (2021). CLytA-DAAO chimeric enzyme bound to magnetic nanoparticles. A new therapeutical approach for cancer patients?. *Int. J. Mol. Sci.* 22, 1477. https://doi.org/10.3390/IJMS22031477.
- [68]. Frenzel, D., Willbold, D., (2014). Kinetic titration series with biolayer interferometry. PLoS One 9, e106882. https://doi.org/10.1371/JOURNAL.PONE.0106882.
- [69]. Pantoja-Uceda, D., Neira, J.L., Saelices, L., Robles-Rengel, R., Florencio, F.J., Muro-Pastor, M.I., Santoro, J., (2016). Dissecting the binding between glutamine synthetase and its two natively unfolded protein inhibitors. Biochemistry 55 https://doi.org/10.1021/acs.biochem.6b00072.
- [70]. Snider, C., Jayasinghe, S., Hristova, K., White, S.H., (2009). MPEx: a tool for exploring membrane proteins. *Protein Sci.* 18, 2624–2628. https://doi.org/10.1002/ PRO.256.
- [71]. Kyte, J., Doolittle, R.F., (1982). A simple method for displaying the hydropathic character of a protein. *J. Mol. Biol.* **157**, 105–132. https://doi.org/10.1016/0022-2836 (82)90515-0.
- [72]. Rizzuti, B., (2022). Molecular simulations of proteins: from simplified physical interactions to complex biological phenomena. *Biochim. Biophys. Acta Proteins Proteom.* 1870 https://doi.org/10.1016/J.BBAPAP.2022.140757.

- [73]. Wang, Z., Pan, H., Sun, H., Kang, Y., Liu, H., Cao, D., Hou, T., (2022). fastDRH: a webserver to predict and analyze protein-ligand complexes based on molecular docking and MM/PB(GB)SA computation. *Brief. Bioinform.* 23 https://doi.org/10.1093/BIB/BBAC201.
- [74]. Tian, C., Kasavajhala, K., Belfon, K.A.A., Raguette, L., Huang, H., Migues, A.N., Bickel, J., Wang, Y., Pincay, J., Wu, Q., Simmerling, C., (2020). ff19SB: amino-acidspecific protein backbone parameters trained against quantum mechanics energy surfaces in solution. *J. Chem. Theory Comput.* 16, 528–552. https://doi.org/ 10.1021/ACS.JCTC.9B00591.
- [75]. He, X., Man, V.H., Yang, W., Lee, T.S., Wang, J., (2020). A fast and high-quality charge model for the next generation general AMBER force field. *J. Chem. Phys.* 153 https://doi.org/10.1063/5.0019056.
- [76]. Izadi, S., Anandakrishnan, R., Onufriev, A.V., (2014). Building water models: a different approach. *J. Phys. Chem. Letters* 5, 3863–3871. https://doi.org/10.1021/ JZ501780A/SUPPL FILE/JZ501780A SI 001.PDF.
- [77]. Kearney, P.L., Bhatia, M., Jones, N.G., Yuan, L., Glascock, M.C., Catchings, K.L., Yamada, M., Thompson, P.R., (2005). Kinetic characterization of protein arginine deiminase 4: a transcriptional corepressor implicated in the onset and progression of rheumatoid arthritis. *Biochemistry* 44, 10570–10582. https://doi.org/10.1021/BI050292M/ASSET/IMAGES/LARGE/BI050292MF00008.JPEG.
- [78]. Neira, J.L., Rizzuti, B., Palomino-Schätzlein, M., Rejas, V., Abian, O., Velazquez-Campoy, A., (2025). Citrullination at the N-terminal region of MDM2 by the PADI4 enzyme. *Protein Sci.* 34 https://doi.org/10.1002/PRO.70033.
- [79]. Holm, A., Rise, F., Sessler, N., Sollid, L.M., Undheim, K., Fleckenstein, B., (2006). Specific modification of peptidebound citrulline residues. *Anal. Biochem.* 352, 68–76. https://doi.org/10.1016/j.ab.2006.02.007.